JONES JR., DERICK D., Ph.D. Molecular Insights into Virulence Regulation in MRSA using Mass-Spectrometry Based Metabolomics. (2020)
Directed by Dr. Nadja B. Cech. 79 pp.

Drug resistant infections are an increasing problem world-wide, with an annual estimate of 300,000 infections a year, 10,000 deaths, and 1.7 billion dollars in costs in the US alone. Current treatment modalities to combat infections of this type rely on antibiotics. Unfortunately, the use of antibiotics accelerates the development of resistance. Severe drug resistant infections such as methicillin-resistant *Staphylococcus aureus* (MRSA) are often managed with "last resort treatments", which have side effects similar to chemotherapy, including, but not limited to, loss of appetite for months at a time, increased hospital stays, and extreme fatigue. MRSA produces a host of toxins that are responsible for its virulence, causing inflammation, skin lesions and, in extreme cases, septic shock and even death. One potential alternative strategy for treating drug resistant bacterial infections would be to inhibit the production of these toxins, thereby making the bacteria less harmful to the host; a so called "anti-virulence" approach. A major advantage of anti-virulence therapeutics would be the ability to reduce the damage caused by bacterial infections without selecting for the development of resistance.

The long-term goal of our research is to develop new anti-virulence strategies against MRSA. With this dissertation, we undertook three projects towards this goal. With Project 1, we developed analytical methodologies to better understand and track virulence in *MRSA* by measuring molecules that are regulated by and regulate the quorum sensing system. With Project 2, we sought to identify new secondary metabolites

produced by MRSA, with a particular focus on those regulated by the quorum sensing system. Lastly, with Project 3, we employed new informatic approaches to identify antimicrobial compounds from the plant *Rumex crispus*. This third project also included a significant training component and was carried out collaboratively with an undergraduate student. A central goal of this dissertation in addition to benchwork science was to recruit and retain a diverse body of students in chemistry. This goal was carried out through effective mentorship and training, as evidenced by the outcomes of Project 3.

MOLECULAR INSIGHTS INTO VIRULENCE REGULATION IN MRSA USING MASS-SPECTROMETRY BASED METABOLOMICS

by

Derick D. Jones, Jr.

A Dissertation Submitted to
the Faculty of The Graduate School at
The University of North Carolina at Greensboro
in Partial Fulfillment
of the Requirements for the Degree
Doctor of Philosophy

Greensboro
2020

Approved by

_____
Committee Chair

To my paternal grandmother, Verna D. Jones…

I am a result of your unconditional love. You have inspired me to be great. I miss you with all of my heart. You have always pushed me to dream, to live, and to love unconditionally. You were my greatest inspiration. When I was with you, I felt unstoppable. The love that you embraced me with is still unmatchable. I have questioned God on so many occasions because I was angry that you left this earth so soon. I am so grateful to have the opportunity to dedicate this dissertation to you.

To my paternal grandfather, Earnest L. Jones…

I will always be grateful for you. You taught me that family should always come first. Your legacy, "JONES EMPIRE," shall live on forever. You always knew what to do. You have invested so much into me. You loved me with a love that had no conditions; I hope that this makes you proud as you take your eternal rest.

To my paternal aunt, Karen D. Jones…

What can I say? I miss you so much. You were taken away from me at such a young age. I have always loved and admired you. You would wear the tallest heels. I know that you would be proud of me. I remember your favorite song, "There's a storm out on the ocean, and it is moving, this ole way. If your soul's not, anchored in Jesus, you will surely drift away." I love you forever, and I hope a piece of this dissertation shows the loving heart you have had for all of humanity.

APPROVAL PAGE

This dissertation, written by DERICK D. JONES JR., has been approved by the following committee of the Faculty of The Graduate School at The University of North Carolina at Greensboro.

Committee Chair _____
Nadja B. Cech

Committee Members _____
Mitchell P. Croatt

_____
Alexander R. Horswill

_____
Daniel A. Todd

_____
Date of Acceptance by Committee

_____
Date of Final Oral Examination

ACKNOWLEDGMENTS

This research was supported by the National Center for Complimentary and Integrative Health under award number 5T32 AT008938 (Ruth L. Kirschstein National Research Service Award Institutional Research Training Grant).

I would like to thank Drs. Daniel A. Todd, Alexander Horswill, and Mitchell P. Croatt for offering their guidance and expertise as committee members throughout this process, Drs. Lindsay K. Caesar and Joshua Kellogg for training in data processing and bioinformatic tools to do metabolomics.. I want to send love and light to the entire Cech lab, including undergraduate students, graduate students, and post-doctoral fellows, for their continuous support.

Thank you Dr. Nadja B. Cech for being such an incredible research mentor for three years and for five years (including time I was not a part of your research group). Thank you for always seeing the very best in me, I remember the email you sent saying that you cannot wait to hood me with my PhD. Though it may not happen as planned, we are creative enough to make sure it is celebrated the same. I could write a book about you, but we know our relationship and it is unbreakable. I am so happy that we both can mess up in front of each other and feel great being corrected. Thank you for teaching me community and what it means to build and be a part of one.

Dean Omar Ali, thank you for teaching me community. I could not have done this without you. I must keep it short, because I can write a novel of our relationship. So grateful for the many collaborations and our future collaborations.

To the entire Jones family, especially my Dad, Derick D. Jones, Sr. thank you all for being there. It has been one of the rockiest journeys, but we have all endured. I love each and every one one of you! I cannot imagine being able to finish without feeling your love. The bond that my dad and I share will remain unbreakable! To my cousin/sister Joanna E. Jones, thank you for all the long nights of listening to me, I could not have carried on without you. To my cousin Janelle King, thank you for always believing in me, thank you for showing up when I needed you most (holistically). Thank you for teaching me that perfection was living in your truth. You held my hand emotionally during one of the toughest times in my life. You have always been a big sister to me. To Kelvin King, I am so happy to have you in my family. Thank you for your push and belief in me.

A very special shout out to Ms. Jacqueline L. Prayer, mom (adopted-step mom) you have always been there for me. When I did not know how to pay for school, you found the money. It is because of you that I have made it this far. Your texts, and the motherly love I feel is so great. From birth until now, thank you! Near or far, you are always in my heart.

To Dean Gregory C. Bell, you have been a mentor to me outside of science. You let me advocate for graduate students. You saw me as a human always, I am so eternally grateful for you. You have always believed that I would complete my PhD, look at where we are now. To Dr. Lake' Buggs, have challenged me in ways that would push me to dig deeper. Thank you for being a black woman with a PhD willing to mentor me outside of your expertise. You both are great people in the academy and mentors for a lifetime. It is because of you I have so many things going for me, outside of the laboratory. To Dean

Kelly Burke of the Graduate school, thank you for your trust in me and my leadership. It has not been easy, but it was worth it. Thanks for the real-life conversations. I am so proud that I am graduating with you as Dean. You have taken so many risks to ensure that graduate education is at its prime. I am just so honored to see you lead. If you ever need anything in life, I will always be there.

To the Graduate Student Association at UNC Greensboro, I am forever grateful to have been able to serve as your Vice President for 2 years and your President for 1 year. We have accomplished so much together. To the UNC System Association of Student Governments, it has been the greatest joy to serve the entire state of NC and advocate for graduate visibility, mental health, and living wages. Thank you for believing in me.

To Chantal V. Pelzer, my first Cech lab mentee. You have accomplished more than you will ever know. It warms my heart to see a Public Health major with a science publication. Please remember I believe in you and will always believe in you for a lifetime. Never stop dreaming. Whenever you need me, I will always be there.

To Dahlia Porter, thank you for allowing me to mentor you this last semester. I am so proud of your progress and I know you will be the independent scientist you so desperately want to be. I want you to remember to "PUSH" even when it seems as if the weight of the world is on your shoulder. Never stop. You are magical and unstoppable.

To my Spiritual leader, Bishop Daniel Walter Rogers, Jr. there is so much I can say, but I will keep it short. Thank you for accepting me and nurturing me back to spiritual health. Thanks for the weekly check-ins and reading my facial expressions. Thank you for allowing me to be my authentic self. I have called you out, as you would

say, a lot, however the greatest gift, is being able to grow! To my Beyond Church Family, I love each and every one of you. You all have prayed and kept me grounded. I am here to stay.

To Dean Sherine Obare, I am your biggest fan. You have cheered for me when it felt as if no one was cheering for me. You kept me rooted and grounded. You have reminded me that getting this PhD is a powerful thing. Thank you for reminding of it. Sooner or later the frustrations in life will be at a table where I am able to speak and be heard. I appreciate you always making time for me!

Lastly, to all the beautiful dreamers, BLACK LIVES HAVE ALWAYS MATTERED, do not let anyone tell you different. To the phenomenal women who have given birth to a nation, I am forever indebted to you. To all the men that have sacrificed so that I can be, thank you! To all my trans and non-binary kindred, thanks for rocking with me and supporting me, and speaking up for me when I was hurting. To all the marginalized people in STEM pursuing a terminal degree, KEEP GOING. The odds are against you, but YOU are built to do it. So much love and light to the world.

TABLE OF CONTENTS

Page

LIST OF TABLES

Page

LIST OF FIGURES

Page

CHAPTER I

INTRODUCTION

Jones Jr., D.D. conducted the literature review and wrote all sections of this chapter.

Antimicrobials and Medicine

It is imperative to understand the role of antibitotics in improving human health. Antibitocits are arguably one of the greatest success stories in the history of medicine. The discovery of antimicrobials started a medical revolution known as the antibiotic era. This chapter provides a brief history of the discovery of some antimicrobials and how many lives were saved since their first serendipitous discovery.

The antibiotic era is usually associated with Alexander Fleming and Paul Ehrlich [1]. Ehrlich's idea of a "magic bullet" that could selectively target only disease-causing microbes and not the host was based on an observation using synthetic dyes like aniline. It was further observed that these dyes could only stain specific types of microbes. Based on these observations, Ehrlich claimed that these chemical compounds could be synthesized and would be able to target the pathogenic microbe [1] exclusively. Ehrlich first described this concept in 1900. Erhlich clearly stated that these chemicals harmed the pathogens and not the host [1, 2]. One of the first "magic bullets" that were successful in treating syphilis was arsphenamine. Through Ehrlic's concept of the magic bullet, the first naturally occurring antimicrobial was discovered [2]. The golden age of the antibiotic era begins when Fleming serendipitously discovered penicillin from a mold

that contaminated his petri dishes while he was conductinginfluenza studies [1-3]. Penicillin was a hallmark for treating infections and diseases associated with *Staphylococcus aureus*. This was great news for the medical field until they noticed that the illnesses were becoming harder to treat because of the resistance it had to begin to develop.

Developing Resistance to Antimicrobials

Staphylococcus aureus is a commensal bacterium that colonizes the normal skin and nasal cavity in approximately a third of the human population [4]. In addition to *S. aureus* commensal characteristics, it can become a pathogen to a human or animal host. This activity meants that it is characterized as an opportunistic pathogen. *S. aureus* causes a wide range of infections, some of the most severe conditions being septicemia and toxic shock syndrome. These infections and associated diseases could be life-threatening if left untreated [4], and *S. aureus* is a leading cause of human bacterial infections worldwide [5]. The Centers for Disease Control had classified *S. aureus* as one of the high priority pathogens, with infection rates in the hundreds of thousands and the deaths in the tens of thousands [6].

S. aureus is a high priority pathogen listed by the CDC because it can develop resistance rapidly to newly developed antibiotics. The go to antimicrobial for *S. aureus* in its multi-drug resistant form is vancomycin, and there are strains resistant to this last resort antimicrobial, making it challenging to treat [6].

S. aureus' unique ability to develop resistance to many antibiotics classes has made it a subject of extensive study. *S. aureus* has many resistant strains, with one being

methicillin-resistant *Staphylococcus aureus* or MRSA [7]. The current treatment modality for this highly antibiotic-resistant pathogen consists of a cocktail of drugs with similar effects to chemotherapy. We have heard patients describe their symptoms concurred with research reviews [8], loss of appetite, extreme fatigue, inability to work, excessive weight loss, and many others. MRSA has become more prevalent in recent years as a community-acquired (C.A.) infection; most infections were hospital-acquired (H.A.). Over the last decades, this CA-MRSA has been the most prominent cause of drug-resistant *S. aureus* infections [9].

Antibiotics that were once active against CA-MRSA are no longer useful, resulting in a need for more antimicrobial drug discovery efforts [8]. Antibiotics kill bacteria through various modes of action, including damage to the cell wall and inhibition of DNA synthesis [8]. The selective pressure applied to bacteria exposed to antibiotics results in the evolution of resistance mechanisms, making many antibiotics ineffective [10]. Increased resistance is, in part, due to the overuse of antibiotics [7, 11].

Need for new ways to treat infections

With this dissertation, we sought to develop methods that would improve our understanding of molecules secreted by MRSA [12, 13] that allow it to thrive in hostile environments. This ability to succeed is often referred to as virulence [14]. It is imperative to seek alternative treatment modalities in conjunction with continuing efforts in antibiotic drug discovery. The first project in this study aimed to develop an analytical methodology to detect known MRSA metabolites, enabling tracking of MRSA growth and virulence. Throughout this dissertation, we sought to employ mass spectrometric

tools to answer these biological questions. Mass spectrometry is one of the most effective technologies for targeted and untargeted analysis, outlined in detail by previous peer-reviewed literature [6, 15-17]. Throughout this dissertation, we detail how mass spectrometric methods were employed to answer questions from a chemical and biological perspective. Using this tool, we made significant progress in identifying unknown virulence compounds or degraded products of virulence products that may have a biological function. Finally, we putatively identified molecules that inhibit bacterial growth from a botanical source, the plant *Rumex crispus*.

Commitment to Mentorship as a way to Increase Diversity

Throughout this dissertation, a significant effort was focused on the recruitment and mentorship of people from underrepresented communities. This effort was made to aid in diversifying science. While progress has been made in the science, technology, engineering, and mathematics (STEM) field is still sorely lacking diversity. Encountering black or brown people with a Ph.D. (or in pursuant of a Ph.D.) is surprising. But to see a black person who is also a part of the LGBTQIA+ community can be disturbing and challenging for students (undergraduates, post-baccalaureate, and advanced degree seekers) who are attempting to get a degree in the same or similar field. Similar to the concept of a syndemic in the epidemiology literature [18], the social sciences have urged us to consider how social context intersects with other variables by offering the framework of intersectionality for our consideration [19]. In short, intersectionality is overlapping or identifying with more than one subgroup of people, and at some point,

they overlap. Fields et al. [19] offer a schematic of intersectionality for our consideration (**Figure 1.1**):

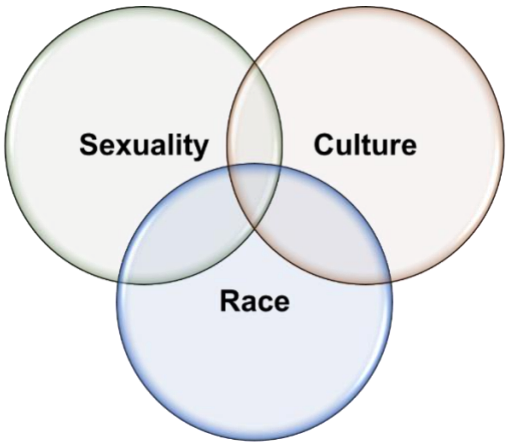

Figure 1.1. Concept of intersectionality visualized. The overlapping of each of the spheres (circles) indicates how these three factors overlap one another (sexuality, culture, and race).

With this knowledge, the mentorship of those not typically seen in the field is of high priority. Chapter IV of this dissertation is a direct result of this commitment.

CHAPTER II

TARGETED AND UNTARGETED ANALYSIS OF SECONDARY METABOLITES TO MONITOR GROWTH AND QUORUM SENSING INHIBITION FOR METHICILLIN-RESISTANT STAPHYLOCOCCUS AUREUS (MRSA)

This chapter has been published in the Journal of Microbiological Methods and is presented in that style. Jones, D. D. Jr.; Caesar, L. K.; Crandall, W. J.; Pelzer, C. V., Jenul, C.; Todd, D. A., Horswill, A. R.; Cech, N. B. J. Microbiol. Met. 2020, 176, 1060000.

Jones Jr., D. D. conceptualization, methodology, investigation, formal analysis, and writing- original draft preparation. Caesar, L. K. helped with supervision of the project, writing- reviewing and editing, and methodology. Pelzer, C. V. helped with investigation, Crandall, W. J. helped with figure preparation, and reviewing and editing. Jenul, C. collaborated with Jones in investigation, writing-reviewing and editing. Todd, D. A. aided in methodology and conceptualization. Horswill, A. R. also helped with conceptualization, methodology, reviewing and editing. Cech, N. B. conceptualization, methodology, resources, supervision, project administration, and funding acquisition.

Introduction

Staphylococcus aureus is a Gram-positive bacterium that colonizes the mucosal membranes and epithelial surfaces of more than 30% of the healthy adult population [20, 21]. *S. aureus* causes infections in both healthy and immunocompromised individuals [14, 22], and methicillin-resistant *S. aureus* (MRSA) is one of the most problematic multi-drug resistant pathogens, responsible for more than 10,000 hospital-acquired annual mortalities in the US alone [6]. While MRSA was originally observed primarily

in hospital settings, over the past two decades, there has been an increase in community acquired MRSA infections [5, 22]. The MRSA strains most commonly associated with community acquired infections are characterized by their hyper-virulence, which results from their production of high levels of toxins that cause inflammation and tissue damage [9]. Thus, it has been suggested that a promising strategy for combating MRSA infections would be targeting toxin production, a so-called "anti-virulence" approach.

Toxin production in MRSA is controlled by two-component regulatory systems, most importantly the accessory gene regulatory (*agr*) system [23, 24]. Activation of this system occurs in a cell-density dependent fashion when an autoinducing peptide (AIP) secreted by the bacteria binds to the extracellular receptor AgrC, a membrane-bound histidine kinase. Binding of AIP to AgrC induces changes in gene expression that ultimately lead to the production of multiple virulence factors, including the phenol soluble modulins (PSMs).

Previous investigations have sought to track virulence in MRSA by measuring quorum sensing regulated metabolites. For example, our group and others have detected the AIPs directly from bacterial culture media [25-29]. Others have reported the detection of outputs of the quorum sensing system such as phenol soluble modulins (PSMs) [30-33] including delta toxins [33-35]. The limitation of measuring these metabolites to monitor virulence is that it is difficult to disentangle anti-virulence activity from anti-microbial activity; inhibition or delay in bacterial growth will have the same effect (decrease in metabolite production) as inhibition of quorum sensing. Prior to the current work, this problem has been addressed by simultaneously monitoring quorum

sensing and tracking bacterial density with OD_{600} readings [26, 36]. With the current study, we sought to develop an alternative strategy, the application of a mass spectrometric method that could simultaneously monitor multiple classes of secondary metabolites produced by MRSA, including metabolites controlled by the *agr* system (as an indicator of virulence) and those that are not (as an indicator of growth).

In conducting this study, we predicted that the aureusimines might be useful metabolites to employ for the purpose of monitoring *S. aureus* growth. Production of aureusimines by *S. aureus* has been independently discovered by the Fischbach and Magarvey research groups [37, 38]. Aureusimine biosynthesis is dependent on the *ausAB* operon, also referred to as *pznAB* operon, which encodes a nonribosmal peptide synthetase (*ausA*) and 4′-phosphopantetheinyltransferase (*ausB*). An early report [38] had suggested aureusimines to be major virulence regulators in *S. aureus*, but a more recent study showed that these regulatory effects were due to a secondary mutation in the SaeRS two-component system[39]. Therefore, the biological role of aureusimines has yet to be determined. With this study, we endeavored to test the utility of tracking aureusimine production as a way to monitor MRSA growth.

Materials and Methods

MRSA culture for monitoring metabolite production over time

Methicillin-resistant *Staphylococcus aureus* (LAC USA300) was used for these experiments [25]. A 24 hr culture was grown in Mueller Hinton Broth (MHB) at 37°C with shaking at 200 rpm using a New Brunswick Scientific shaker/incubator series I-26. The culture was diluted into triplicate borosilicate glass Erlenmeyer flasks containing 150

mL of MHB at a dilution of 3.7×10^8 CFU (colony forming units). Every 2 hr, a 500 µL aliquot was removed from each flask and the OD_{600} was measured. Also, at each time point a second aliquot was removed, filtered with a 0.22 µm centrifugal filter with a polyvinylidene difluoride (PVDF) membrane, and the filtrate was retained for analysis with ultraperformance liquid chromatography-mass spectrometry (UPLC-MS).

MRSA culture for growth and quorum sensing inhibition

A slight modification of a previously described method was used to evaluate the influence of inhibitors on MRSA metabolite production [40]. Briefly, MRSA (LAC USA300) was cultured at 37 °C in tryptic soy broth (TSB) for 24 hr with shaking at 200 rpm in a New Brunswick Scientific shaker/incubator series I-26. This culture broth was diluted 1:100 in TSB and cultured with shaking at 200 rpm at 37 °C for 2 hr, at which point the OD_{600} was measured to be in the range of 0.08-0.1. A 96-well tissue culture treated flat bottom plate (Corning Incorporated) was inoculated with 245 µL of this diluted bacterial inoculum and 5 µL of inhibitor or control in each well. The inhibitors included ambuic acid (Adipogen life Sciences) and chloramphenicol (Sigma Aldrich) at assay concentrations of 0.77 µM to 100.00 µM and 2.34 µM to 300.00 µM, respectively. Stock solutions of ambuic acid and chloramphenicol were prepared in DMSO and assay content of DMSO was 2% in all wells. Assays were performed in triplicate for each treatment and control. The vehicle control consisted of 2% DMSO. The plate was incubated at 37 °C and shaken at 1000 rpm in a Stuart Microtitre Shaker Incubator (SI505). OD_{600} was measured at 1 hr intervals using a Synergy H1 Plate Reader and the experiment was considered complete at OD_{600} of 2.0 (~4-6 hr). At completion of the

incubation time, the culture broth containing bacteria was transferred to a clear sterile 96-well, 0.22 µm hydrophilic plate with low protein binding durapore membrane (MultiScreen®) and filtered under vacuum. The spent media were then analyzed by UPLC-MS.

MRSA culture for experiments with deletion mutants

Three strains of MRSA were used in these experiments, a clinical isolate referred to as MRSA LAC USA300 (AH1263) [41] and a genetic deletion mutant engineered to knock out aureusimine production (AH2137), and a genetic deletion mutant engineered to knock out the *agr* quorum sensing system (AH1292) [35]. Triplicate samples of a diluted 24 hr inoculum (prepared as described in MRSA culture for growth and quorum sensing) of each strain (30 mL total volume) were cultured in MHB in 50 mL falcon tubes for 24 hr with shaking at 200 rpm at 37 °C. At the 24 hr time point, each culture was filtered with a centrifugal filter (PVDF) and the spent medium was analyzed by UPLC-MS.

To construct the AH2137 *ausA* deletion plasmid, homology arms (~1100 bp) upstream and downstream of *ausA* were amplified with primer pairs (IDT) CLM508/CLM512 and CLM510/CLM511 (**Table 2.1**). The PCR products were column purified with the QIAquick PCR purification kit (Qiagen) and fused in a second PCR with primers CLM508 and CLM511. The PCR product was gel purified with the QIAquick gel extraction kit (Qiagen), digested with SacI and SalI (New England BioLabs Inc), and ligated into plasmid pJB38 [42] digested with the same restriction enzymes to generate plasmid pCM44. The plasmid was electroporated [43] into strain RN4220 [44] and clones carrying pCM44 were selected on TSA plates containing chloramphenicol (Cm, 10

µg/ml) at 30 °C. The plasmid was recovered with the QIAprep Spin Miniprep Kit (Qiagen) from overnight cultures grown at 30 °C in TSB containing Cm (10 µg/ml) and sequenced with primers SEQ, REVCOMPSEQ and SEQ62D. The plasmid was then electroporated into USA300 strain LAC, clones carrying pCM44 were selected on TSA plates containing Cm (10 µg/ml) and individual colonies were subsequently streaked on TSA plates containing Cm (10 µg/ml) and incubated at 42°C to select for integration into the chromosome. Single colonies were grown in TSB at 30°C with shaking and diluted 1:500 in fresh media for four successive days before diluting to 10^{-6} and plating on TSA containing 200 ng/ anhydrotetracycline to select for loss of the plasmid. Colonies were screened for resistance to Cm, and Cm^S colonies were screened by PCR for deletion of *ausA.*

Table 2.1. Primer list

Primer Name	**Primer Sequence [a, b]**	**Restriction site**
CLM508	GTTGTTGAGCTCGGTTACCTCAAGACCGAAATCAAG	SacI
CLM512	**TGCGCAGTACTTGCTACCATGG**CTCATTACTTACTGAAATTGCATG	
CLM510	C**CATGGTAGCAAGTACTGCGCA**GTAAGTAGGGAAAGTTATGACAG	
CLM511	GTTGTTGTCGACCACTGACTAACATTAACGTGAG	SalI
SEQ	CATGCAATTTCAGTAAGTAATGAG	

REVCOMP SEQ	CTCATTACTTACTGAAATTGCATG	
SEQ62D	CTCACGTTAATGTTAGTCAGTG	

a. Restriction sites are underlined
b. Linkers are indicated in **bold**

UPLC-MS analysis

An Acquity UPLC system (Waters, Corporation, Milford, MA) coupled to an LTQ-Orbitrap XL hybrid mass spectrometer (Thermo Fisher Scientific, Waltham, MA) was used for UPLC-MS analyses. For the samples collected in the 24 hr growth analysis (*Section 2.1*) a 3 µL injection of each sample was eluted from the column (Acquity UPLC BEH C18 1.7 um, 2.1 x 50 mm, Waters Corporation) at a flow rate of 0.3 mL/min with solvent A consisting of water (Optima LC-MS grade) with 0.1% formic acid added and solvent B consisting of methanol (Optima LC-MS grade). The gradient was initiated with an isocratic composition of 60:40 (A:B) for 0.5 min, increasing linearly from 0.5 min to 7.50 min to 30:70 (A:B) followed by an isocratic hold for 0.5 min. From 8.0-8.5 min the gradient increased linearly to 0:100 with a 0.5 min isocratic hold. The gradient returned to initial starting conditions from 9.0-9.5 min and was held for 0.5 min. The mass spectrometer was operated in positive ion mode for the scan range of 150-1500 with the following settings: capillary voltage of 5 V, capillary temperature of 300 °C, tube lens offset of 35 V, spray voltage of 3.80 kV, sheath gas flow of 35, and auxiliary gas of 20. The same method was employed for samples from the growth inhibition studies (*Section 2.2*) and deletion mutant experiments (*Section 2.3*) except that a different column

(Acquity UPLC BEH SHIELD RP C18 1.7 um, 2.1 x 50 mm, Waters corporation) was used.

To identify selected MRSA metabolites, MS-MS analysis was conducted using collision-induced dissociation (CID) with a collision energy of 35.0. Fragmentation patterns, retention times, and accurate masses were compared between putative metabolite signals in the MRSA culture medium and data for standards for AIP-I (Anaspec), δ-toxin (Anaspec) and aureusimine B (Cayman chemicals). Data dependent acquisition was employed with an inclusion list for the masses of 961.3798 (AIP-I), 229.1332 (aureusimine B) and 752.4135 (δ-toxin). A calibration curve was also collected for the AIP-I standard to establish the linear range of instrument response, using a concentration range of 1.0×10^{-4} to 1.0×10^{1} μg × mL^{-1}.

All mass spectrometric data have been made publicly available through MassIVE (MassIVE ID: MSV000085457, **doi:** 10.25345/C5WT5R, https://massive.ucsd.edu/ProteoSAFe/dataset.jsp?accession=MSV000085457).

Untargeted metabolomics procedures

`Untargeted metabolomics data analysis was conducted on the mass spectrometric data for samples generated in the growth inhibition studies (*MRSA culture for growth and quorum sensing inhibition*). Mass spectrometric data were analyzed, aligned and filtered with MZmine 2.2 software (http://mzmine.sourceforge.net/) [45]. The parameters can be found in **Table2.2.** Briefly, peak detection in MZmine was obtained above a baseline of 1.2×10^{6} and a chromatogram was constructed for each of the *m/z* values that spanned longer than 0.1 min. The deconvolution parameters for peak detection included noise

level (absolute value) at 1.2×10^6, minimum peak duration 0.5 min, tolerance for *m/z* variation 0.001 and tolerance for *m/z* intensity variation 10%. The join aligner algorithm was used to create a compiled peak table by setting the balance between *m/z* and retention time at 10.0 each, *m/z* tolerance at 0.05, and retention time tolerance as 2 min. The spectral data matrix was imported to Excel (Microsoft, Redmond, WA, USA) and the OD_{600} data were included to form a final data matrix. Using optical density (OD_{600}) as the dependent variable, we conducted multivariate statistical analysis to construct 4-component partial least squared scores and loadings plots. From the univariate model, selectivity ratio analysis was conducted using Sirius 10.0 (Pattern Recognition Systems AS, Bergen, Norway). This approach was used to identify which features of the dataset (detectable ions/independent variables) were correlated with growth.

Table 2.2. Parameters used for UPLC-MS analysis.

Noise level (absolute value)	1.2×10^6
Minimum peak duration	0.5 min
Tolerance of *m/z* variation	0.001
Tolerance for *m/z* intensity variation	20%
Balance between retention time and *m/z*	10
m/z tolerance	0.05
Retention time tolerance	2 min

Results and Discussion

Untargeted metabolomics of a growth curve to detect MRSA metabolites

To inform the selection of analytes for targeted mass spectrometric analysis, we first conducted untargeted mass spectrometry metabolomics experiments. Critical in these experiments was the application of a data analysis tool, the selectivity ratio, which enables complex mass spectrometric datasets to be simplified by identifying features associated with a given dependent variable [6, 46, 47]. Using untargeted metabolomics with selectivity ratio analysis, we sought to identify specific MRSA metabolites that could be detected as increasing in abundance with increasing OD_{600}.

Untargeted metabolomics analysis of MRSA cultures is complicated by high levels of background introduced by the rich culture medium. This high level of background makes it difficult to distinguish the signals for MRSA metabolites of interest from spurious signals resulting from the culture medium. To resolve this issue, we analyzed a time-dependent series of MRSA cultures using UPLC-MS and conducted untargeted metabolomics analysis of the combined dataset. We then employed selectivity ratio analysis [48] to determine which features in the metabolomics dataset were correlated with bacterial growth (as measured by OD_{600}) (**Figure 2.1**). The selectivity ratio serves as a ranking tool, indicating which features are more likely to be associated with the dependent variable (in this case growth). For a given study, the investigator may select a selectivity ration cut-off value for which features to include in the dataset. This cut-off value can be adjusted up or down depending on the research question being asked. For the studies described herein, a selectivity ratio cut off of 0.36 was selected because

all of the known MRSA metabolites had selectivity ratios greater than or equal to this value.

In **Figure 2.1**, features (*m/z* retention time pairs) that correlate with growth (OD_{600}) are indicated by positive selectivity ratios. Of the 2090 features detected above a signal intensity of 1.2×10^6 with untargeted UPLC-MS metabolomics across the twelve timepoints of the growth experiment, only 5% had selectivity ratios above 0.36, more than half of these (49 ions) were putatively identified as isotopes, multiply charged ions, or adducts associated with seven known MRSA metabolites based on accurate mass values reported in the literature (**Table 2.3**). The known metabolites for which ions were detected in the untargeted metabolomics analysis include aureusimines A and B, AIP-I, formylated and deformylated δ – toxin, phenol soluble modulin (PSM) α-2 and PSMα-3 (see ions color coded and labeled in **Figurer 2.1**). In addition to the expected known MRSA metabolites, a number of additional features were detected among the top 5% of ions with highest selectivity ratios (shown unlabeled in grey in **Figure 2.1**). These features could be unidentified adducts, fragments, or charge states of known metabolites or could correspond to hitherto unidentified MRSA metabolites. Future studies to assign structures to the unidentified features would be of interest. The data in **Figure 2.1** illustrate the utility of selectivity ratio analysis as a methodology for interpreting untargeted metabolomics data; it is far simpler to find 49 relevant features from among 87 features, than from the total of 2090 features. Additionally, the number of potential relevant unidentified metabolites is greatly reduced using the selectivity ratio analysis.

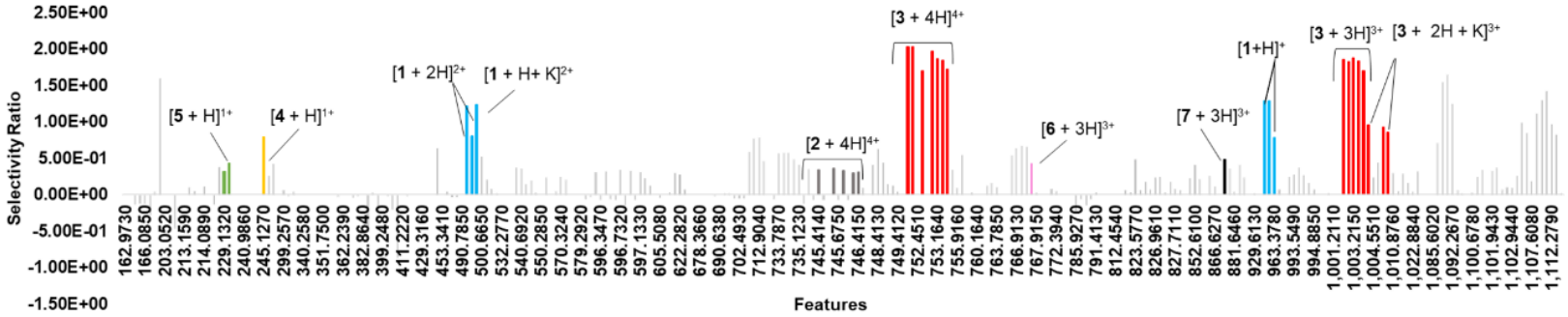

Figure. 2.1. Histogram showing selectivity ratio (SR) for each feature in the untargeted metabolomics dataset for the 24-hour growth experiment shown in Figure 2.2. The MRSA was sampled every two hr and the metabolite profiles for each time point collected using UPLC-MS. OD_{600} measurements (indicating bacterial growth) at each timepoint were used as the dependent variable in calculating the selectivity ratio. The x-axis represents the feature (identified by its *m/z*) detected in the metabolomics dataset. Features are shown in order of increasing *m/z*. Peaks are numbered to correspond with known metabolites that were detected as shown in **Table 2.3**. Higher selectivity ratio indicates stronger correlation with growth (as measured by OD_{600}). 87 features had selectivity ratios above 0.36, 49 of which were putatively identified as ions associated with 5 known MRSA metabolites.

Table 2.3. Known secondary metabolites produced by MRSA indicating structure and function. All compounds were tentatively identified in the MRSA cultures based on accurate mass measurement (**Table 2.4**), as shown in **Figure 2.1**.

Name	***Id #***	***Structure/Sequence***	***Monoisotopic Mass***	***Function***	***Reference***
Autoinducing Peptide-I (AIP-I)	**1**	YSTc(CDFIM)	960.3720	signaling peptide for the *agr* system	[4, 26, 49, 50]
δ-toxin	**2**	MAQDIISTIGDLVKWIIDT- VNKFTKK	2977.6277	*agr-regulated* virulence factor	[31-33, 35]
Formylated δ-toxin	**3**	fMAQDIISTIGDLVKWIIDT- VNKFTKK	3005.6297	*agr-regulated* virulence factor	[31-33, 35]
Aureusimine A	**4**	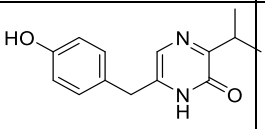	244.1207	function undetermined	[37, 51]
Aureusimine B	**5**	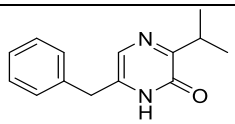	228.1257	function undetermined	[37, 52]
PSMα-2	**6**	fMGIIAGIIKFIKGLIEKFTGK	2305.3685	*agr-regulated* virulence factor	[30, 32, 33]
PSMα-3	**7**	fMEFVAKLFKFFKDLLGKFLGNN	2633.4080	agr-regulated virulence factor	[30, 32, 33]

Confirmation of detection of known MRSA metabolites

The structural assignments indicated in **Figure 2.1** are only tentative, relying on accurate mass measurement alone (**Table 2.4**). To provide a more rigorous confirmation of structure, correct identification of several of the known MRSA metabolites labeled in **Figure 2.1** was confirmed by comparing accurate mass (**Table 2.4**), retention time (**Figure 2.1**), and MS-MS fragmentation data (**Figure 2.2, 2.3 and 2.4**) to that of available standards and previous literature. Additional confirmation was provided by comparison with an *agr* deletion mutant and a Δ*ausA* deletion mutant (**Figure 2.5**)**.** The *ausA* gene encodes a nonribosomal peptide synthetase that is essential for the biosynthesis of aureusimines [37, 38] hence the Δ*ausA* deletion mutant is deficient in aureusimine production. The data for the mutants display the expected findings, AIP-I and δ-toxin are not produced in the *agr* mutant, and aureusimine B is not produced in the Δ*ausA* deletion mutant. The findings summarized in **Figure 2.6** provide confirmation of correct structural assignment for the subset of metabolites indicated in **Table 2.3** for which relevant standards and mutants were available.

Table 2.4. Calculated and measured masses of known metabolites produced by MRSA.

Identification Number	Compound Name	Charge State	Calculated	Measured	Δppm
1	AIP-I	$[M + H]^{1+}$	961.3798	961.3790	-0.8321
2	Formylated δ-toxin	$[M + 4H]^{4+}$	752.4135	752.4153	2.3923
3	deformylated δ-toxin	$[M + 4H]^{4+}$	745.4135	745.4153	2.3923

4	Aureusimine A	$[M + H]^{1+}$	245.1285	245.1275	-4.0795
5	Aureusimine B	$[M + H]^{1+}$	229.1332	229.1335	1.3093
6	PSM α-2	$[M + 3H]^{3+}$	769.4640	769.4604	-4.6786
7	PSM α-3	$[M + 3H]^{3+}$	586.4314	586.4288	-4.4336

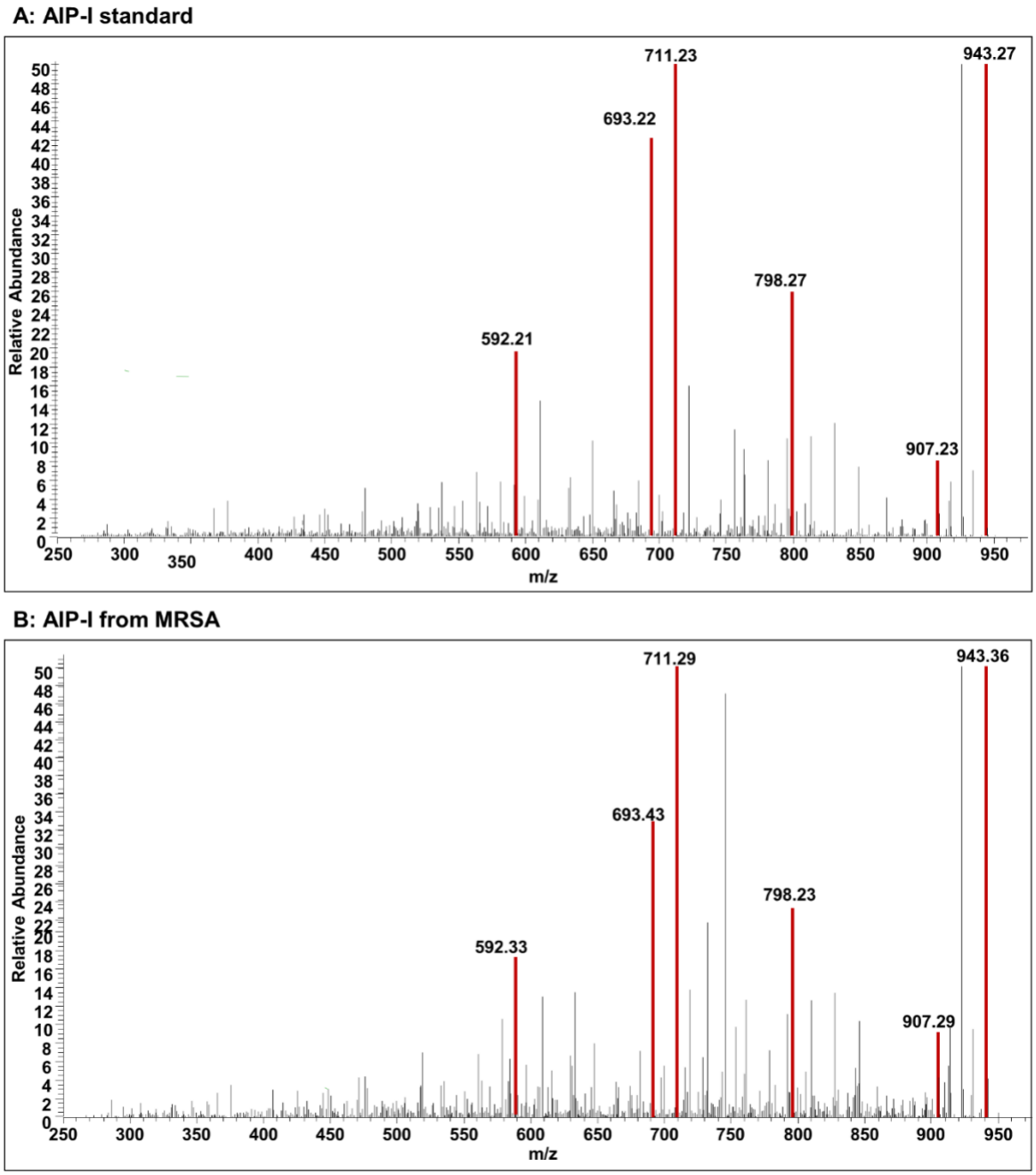

Figure 2.2. MS/MS data of know MRSA metabolites. (A) AIP-I standard and (B) AIP-I bacterial culture. A precursor ion *m/z* of 961.3798 was employed to generate the data for AIP-I.

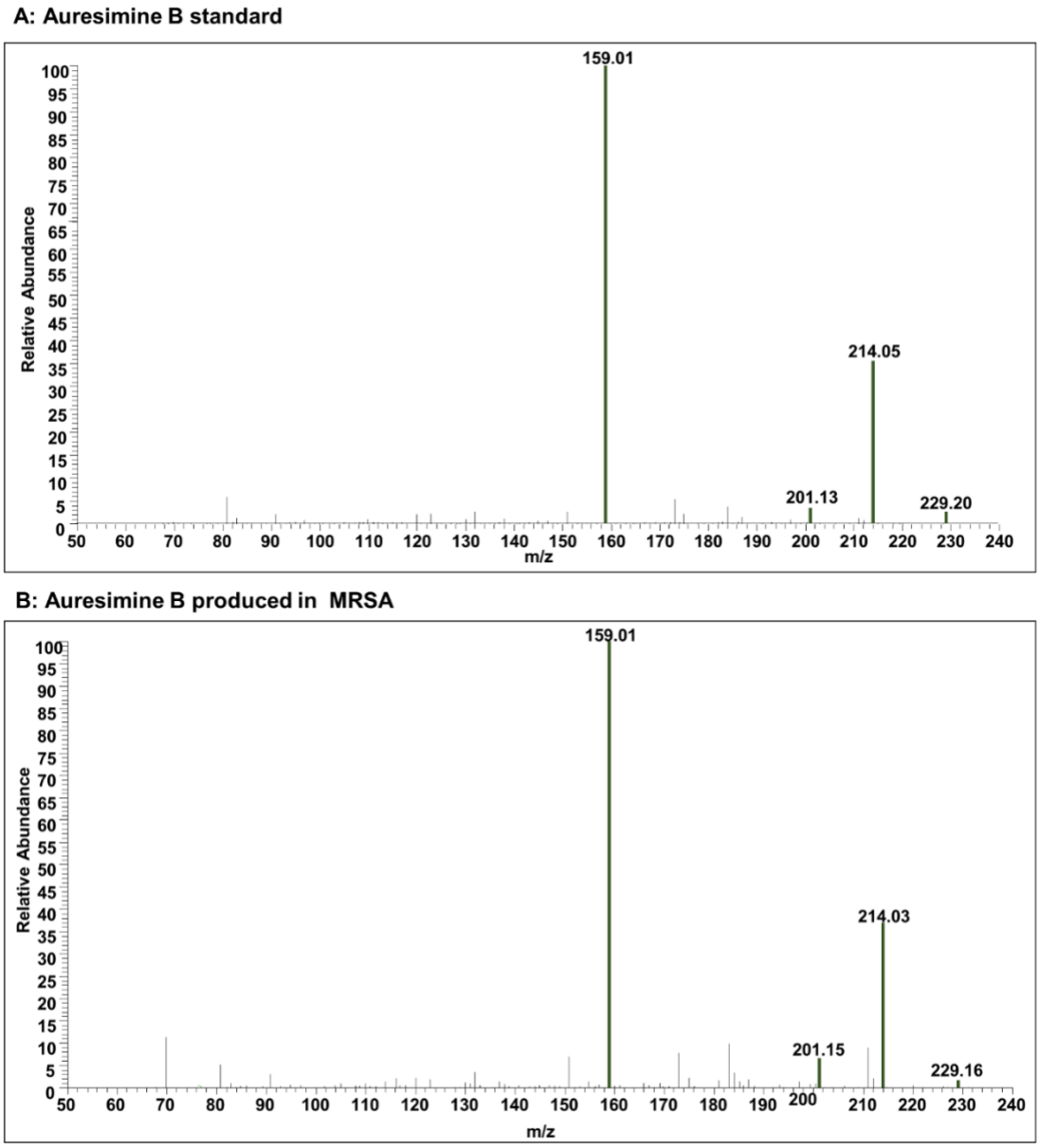

Figure 2.3. MS/MS data of know MRSA metabolites. (A) aureusimine B standard and (B) aureusimine B in bacterial culture. A precursor ion *m/z* of 229.1332 was employed to generate the data for AIP-I.

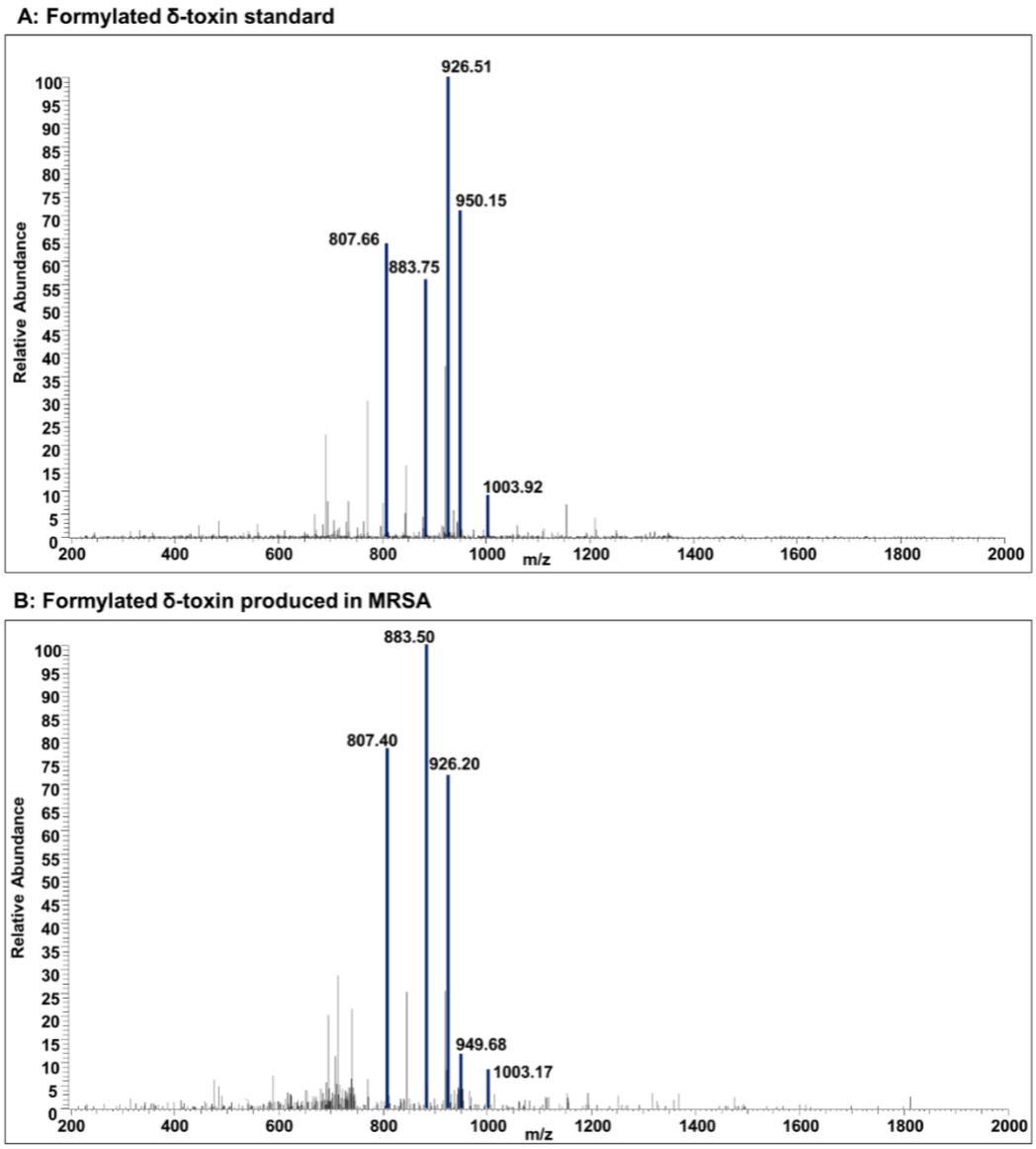

Figure 2.4. MS/MS data of know MRSA metabolites. (A) formylated δ-toxin standard and (B) formylated δ-toxin in bacterial culture. A precursor ion *m/z* of 229.1332 was employed to generate the data for AIP-I.

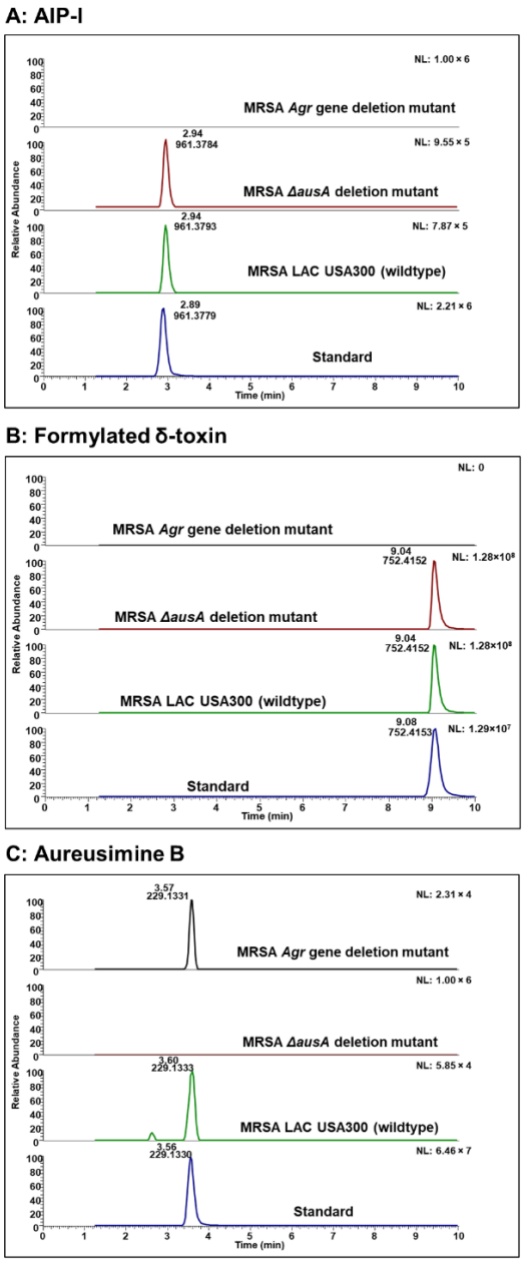

Figure 2.5. Comparison of selected ion chromatograms from targeted UPLC-MS analysis of MRSA metabolites (numbered as in Table 2.3). Data are shown for a clinical isolate of MRSA (LAC USA 300 strain AH1263), a Δ*ausA* non-ribosomal peptide synthetase (NRPS) deletion mutant (AH2137), and an *agr* gene deletion mutant (AH1292). The data in (A) compare retention time and mass for an AIP-I standard (*m/z* 961.3798, $[M+H]^+$) with the putative AIP-I ion in the MRSA cultures. The data shown in (B) compares formylated δ-toxin production (*m/z* 752.4135 for $[M+4H]^{4+}$) across all

strains of MRSA and demonstrate agreement in retention time and mass with the standard. Panel (C) shows a comparison of aureusimine B production (*m/z* 229.1332 for $[M+H]^+$) across all strains. As expected, the same metabolites were detected for the aureusimine gene deletion mutant with the exception of aureusimines, which are absent. For the *agr* gene deletion mutant, metabolites regulated by the *agr* system (AIP and δ-toxin) are not detected.

Comparison of OD600 and mass spectrometric methods for monitoring bacterial growth

The newly developed method for detecting MRSA metabolites was employed to track metabolite production over time **(Figure 2.6**). Bacterial growth was monitored using the standard method of OD_{600} (optical density at 600 nm) measurements (**Figure 2.6A**) while at the same time peak areas for metabolites of interest, AIP-I (**Figure 2.6B**), aureusimine B (**Figure 2.6C**) and formylated δ-toxin (**Figure 2.6D**) were also measured. Growth studies show that as the bacterial population increases (as measured by increase in OD_{600}), abundance of individual known MRSA metabolites from different classes also increases (**Figure 2.6**). It is furthermore apparent that the time point at which each metabolite is first detected varies among the metabolites, AIP-I and aureusimine B were first detected at the four hr time point (**Figure 2.6B** and **C**), whereas formylated δ-toxin (**Figure 2.6D**) was not detected until 12 hr. The differences in onset time for production of AIP-I and δ-toxin are expected based on gene regulation with the *agr* system in MRSA, which has been well described in the literature ([24]). The promoter driving AIP-I biosynthesis functions at a low constitutive level, and the promoter driving δ-toxin expression strictly depends on AIP-I signal accumulation.

It is also apparent from **Figure 2.6** that metabolite production levels off in the latter part of the time course experiment. This is presumably due to reduced metabolite

production, although degradation of the metabolite would also cause an apparent leveling in production and cannot be ruled out. Differences in the time at which signal levels off is observed between the various metabolites (**Figure 2.6**). While AIP-I levels saturate quickly (after just 6 hr) (**Figure 2.6B**), aureusimine B (**Figure 2.6C**) production continues to increase up to 16 hr, even after saturation has been observed in OD_{600} (**Figure 2.6A**). The reason for the observed saturation in AIP response is biological (decreased production by bacteria or degradation of signal) not methodological (response in the mass spectrometer saturated at high concentrations). A calibration curve of mass spectrometric peak area versus AIP concentration is linear up to a peak area of 1×10^8 (**Figure 2.7**), while saturation in AIP signal is observed in **Figure 2.6B** at a response in the range of 8×10^5.

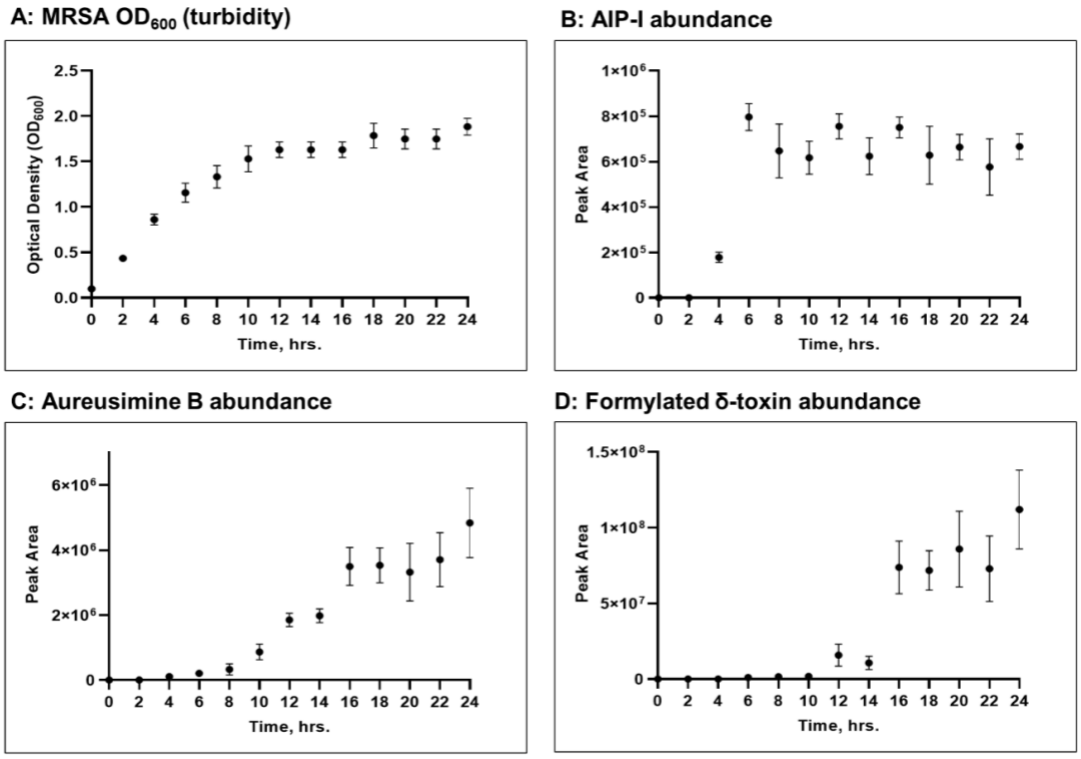

Figure 2.6. Change in abundance of metabolites produced by a USA 300 clinical strain of MRSA over time. MRSA growth was measured by turbidity (OD_{600}) (A). In parallel, abundance of each metabolite was measured every two hr over a 24 hr time period using UPLC-MS. Signal for each metabolite was measured using the area under the curve of the selected ion chromatogram for the relevant ion, AIP-I (B), with *m/z* of $[M+H]^+$ at 961.3798, aureusimine B (C) with *m/z* of $[M+H]^+$ at 229.1332 *m/z*, formylated δ - toxin (D) with *m/z* of $[M+4H]^{4+}$ at 752.4122.

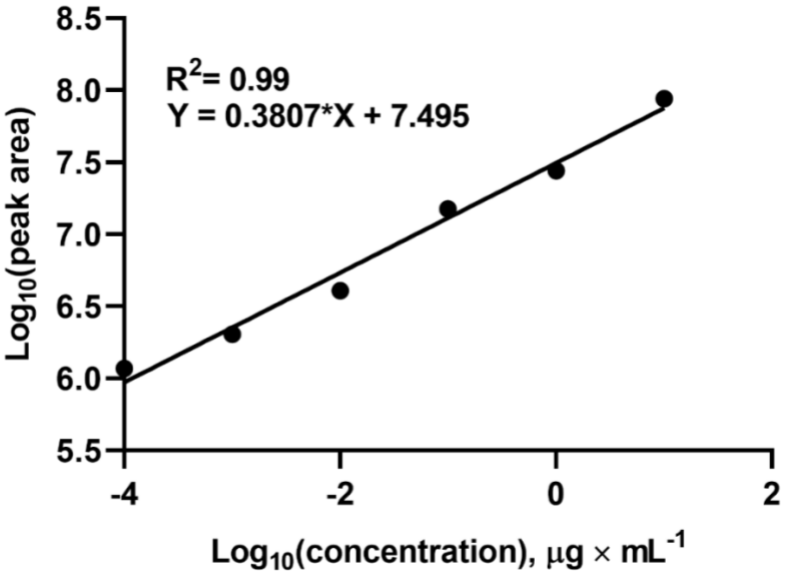

Figure 2.7. Calibration curve of auto-inducing peptide-I. Concentration range 1.0 × 10^{-4} – 1.0 × 10^{1} μg × mL^{-1}

Targeted analyses of known metabolites in response to treatment with an antimicrobial or quorum quencher

Building on the demonstrated ability of the newly developed method to simultaneously track the production of several metabolites associated with virulence of MRSA (AIP-I and formylated δ-toxin), we sought to demonstrate its applicability to track *agr* regulated quorum sensing inhibition. Ambuic acid has previously been shown to act as an inhibitor of the *agr* system [36], while chloramphenicol is a well-known bacterial protein synthesis antibiotic [53]. Therefore, we monitored the influence of these compounds on metabolite production by MRSA across a range of concentrations. Consistent with its antimicrobial activity, chloramphenicol treatment inhibited the production of the three measured metabolites (**Figurer 2.8 B**, **D**, and **F**). Also as expected, ambuic acid inhibited production of AIP-I by MRSA in a dose-dependent

fashion (**Figure 2.8A**). Suppression of AIP-I production should also result in decreased production of other secondary metabolites that are outputs of the quorum sensing system, including δ-toxin. This expected result is observed in **Figure 2.8C**. Consistent with previous literature [36], the observed suppression of AIP-I and formylated δ-toxin by ambuic acid treatment was not due to growth inhibition or growth delay. These experiments were conducted using a short incubation time (6 hr) established previously [36], which achieves rapid MRSA growth by shaking at a high RPM. As demonstrated in the growth curves that accompany **Figure 2.6** (**Figure 2.9**), stationary phase was reached in the 6 hr incubation period, and ambuic acid caused no decrease in OD_{600} up to 100μM (**Figure 2.9**).

In tandem with the quorum sensing inhibition measurements, we sought to employ the mass spectrometric method to monitor growth inhibition. Several ions were identified based on the untargeted metabolomics experiments that could serve as candidates for tracking growth. These ions were detected at *m/z* values of 198.0868, 229.1332, 245.1285, 815.4288 and 871.4870 in positive ion mode mass spectrometry. Among these, only aureusimine B (*m/z* 229.1332) and aureusimine A (*m/z* 245.1285) were identified as known constituents of MRSA. While the other ions appear to be MRSA constituents, their identities are currently unconfirmed. The MS signal for aureusimine A was much lower than that of aureusimine B, making it less desirable for tracking MRSA growth. Therefore, we focused these studies on aureusimine B. Under the conditions employed herein, it appeared that aureusimine B was not strongly regulated by the *agr* system (**Figure 2.8E**).

The data in **Fig 2.8E** suggest that aureusimine B production could be used as a means to track MRSA growth, and that, at least under the conditions employed in this study, the production of this metabolite appears not to be altered in the presence of a quorum sensing inhibitor. Thus, by tracking *agr* regulated metabolites and aureusimine B simultaneously with UPLC-MS, it is possible to measure quorum sensing inhibition and rule out growth interference.

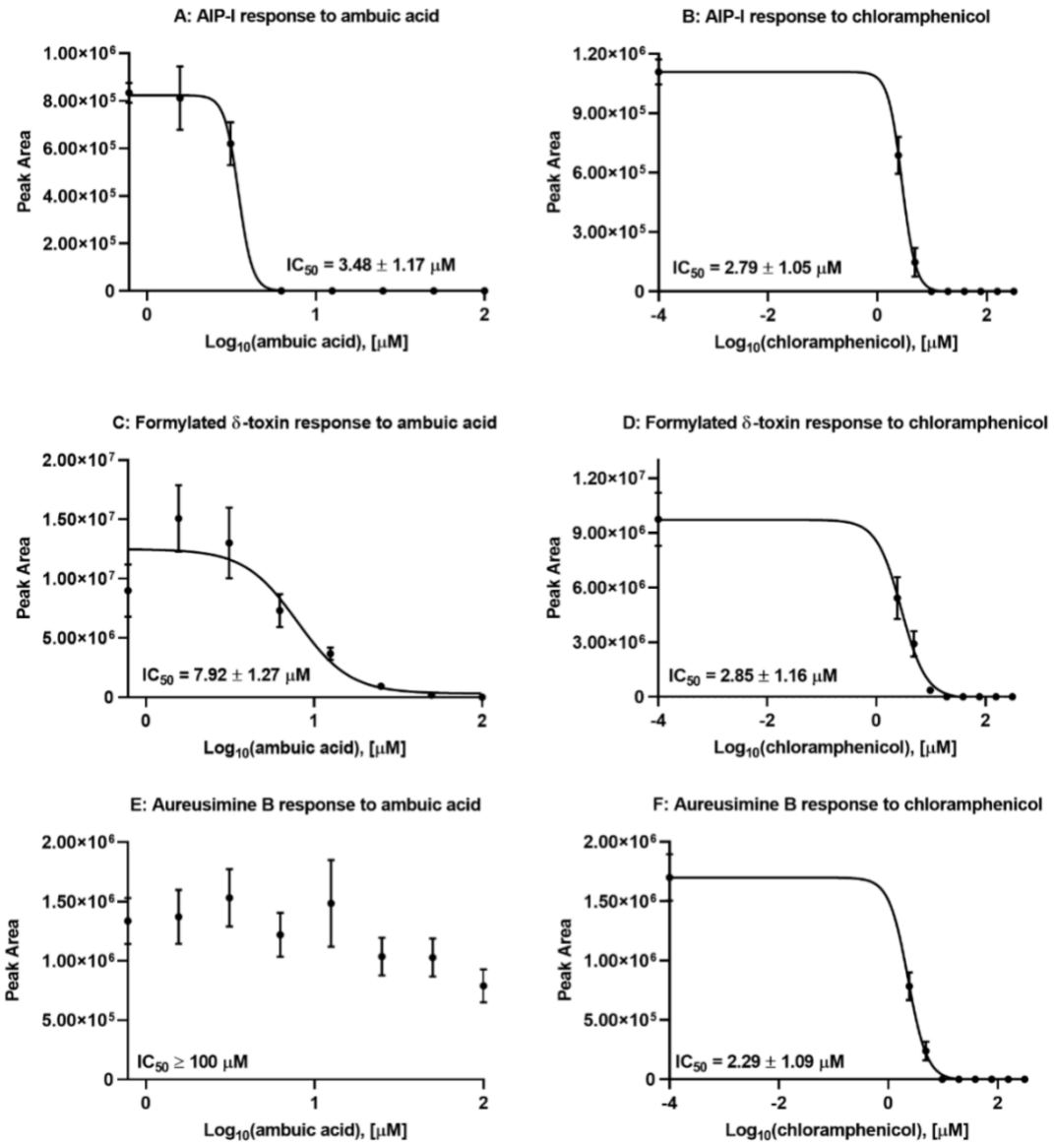

Figure 2.8. Logarithmic dose inhibitory response of known MRSA metabolites to treatment with the quorum sensing inhibitor ambuic acid (A,C, and E) or the antimicrobial chloramphenicol (B, D and F). Masses of the individual ions are indicated in **Table 2.3**. All peak areas were calculated as the average of triplicate cultures. Error bars represent the standard error of the mean. All metabolites decrease in abundance when treated with the antimicrobial chloramphenicol, while only the *agr* regulated metabolites (AIP-I and formylated δ-toxin) respond to treatment with ambuic acid. Data were all collected when the bacterial cultures had reached stationary phase after a 6 hr incubation period. Accompanying growth curves are provided in **Figure 2.9**. IC_{50} values indicate the concentration at which the measured response (peak area) is reduced by 50%.

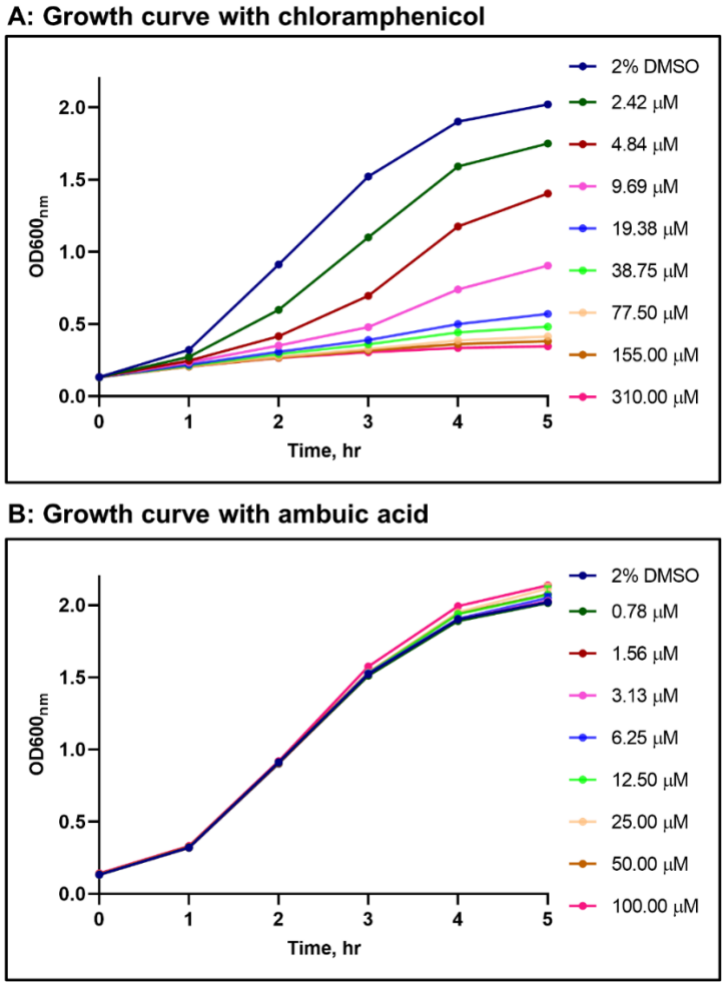

Figure 2.9. MRSA growth curves. (A) Growth curves for MRSA USA300 LAC (AH1263) treated with chloramphenicol over time. Each colored line represents either a control (2% DMSO) or a specific concentration of chloramphenicol. (B) Growth curves for the same MRSA strain shown in (A) treated with ambuic acid at indicated concentrations

Conclusion

With this study, we demonstrate that UPLC-MS can be employed to simultaneously monitor production of multiple secondary metabolites produced by MRSA. To our knowledge, this is the first study to use a single mass spectrometric

method to track both growth and *agr* regulated virulence. We show that aureusimine B production is correlated with bacterial growth, and that by monitoring aureusimine B production in tandem with the production of *agr*-regulated metabolites, it is possible to distinguish the effect of *agr* quorum sensing inhibitors and compounds from those that simply inhibit bacterial growth. The method developed herein could be of benefit to researchers who seek to obtain a more nuanced representation of how metabolite production changes over time or in response to the addition of inhibitors than is provided by OD_{600} data alone. Additionally, this approach could be expanded to have utility in situations where OD_{600} readings are not possible, for example in measurements of bacterial growth *in situ* on surfaces.

Acknowledgments

Funding for this research was provided by the National Institutes of Health, National Center for Complementary and Integrative Medicine, as fellowships to DDJ and LKC (grant number T32 AT008938) and by the National Institute of Allergy and Infectious Diseases (grant number R21 AI133089) to NBC and ARH. ARH was also funded by Merit Award BX002711 from the Department of Veterans Affairs. Mass spectrometry data were collected in the Triad Mass Spectrometry Facility at the University of North Carolina Greensboro.

CHAPTER III

BIOCHEMOMETRICS TO IDENTIFY UPLC-MS FEATURES ASSOCIATED WITH MRSA QUORUM SENSING SYSTEM

This work is under preparation for publication. Derick D. Jones, Jr. conceptualization, methodology, prepared the first draft of chapter . They have made all figures and Tables for this chapter. Cech, N.B. had provided significant guidance, editing and worked collaboratively to write the introduction. Cech, N. B. and Jones, Jr., D.D. both worked to outline this chapter of the dissertation.

Introduction

The history of bacterial infections and their threat to humanity can be categorized with some of the first noted pandemics [54]. The ability of bacteria to evolve and develop mechanisms of resistance has increased the morbidity and mortality resulting from bacterial infections. Opportunistic pathogens such as methicillin-resistant *Staphylococcus aureus* (MRSA) have become resistant to some of the most aggressive antibiotics known to date. One potential cause of this Gram-positive bacterial pathogen, amongst many other pathogens, developing resistance is through the overuse of antibiotics. It has been suggested that the overuse of antibiotics has accelerated the development of resistance. As a result, many of these infections rely on last resort treatments, which involves a cocktail of antibiotics, whose side-effects are comparative to chemotherapeutic cocktails. There is an increasing need to find new approaches to treating drug-resistant bacterial infections. One strategy is the so called “anti-virulence” strategy, which focuses on inhibiting the pathogenicity of the bacterial pathogen. The pathogenicity of

Staphylococcus aureus is a result of its ability to produce high levels of toxins that cause inflammation and cell damage in its host [12]. Toxin production in *Staphylococcus aureus* is controlled by two component regulatory systems [24]. The accessory gene regulator (*agr*) system, also called the quorum sensing system, is one of the key two-component regulatory systems in *Staphylococcus aureus* [23, 24]. The *agr* system is regulated via bacterial cell density. Activation of the *agr* system occurs when an autoinducing peptide (AIP) secreted by the bacteria binds to the extracellular receptor AgrC, a membrane- bound histidine kinase. Once activated by the external stimulus, the sensory protein goes through autophosphorylation, whereby the phosphoryl group that was once attached to the highly conserved histidine residue on the AgrC is transferred to the conserved aspartate residue on the response regulator, AgrA [55]. AgrD is the AIP pro-peptide. It contains a cyclic thiolactone ring and an amphiphatic C-terminal tail which is cleaved upon activation of the quorum sensing system. The protein AgrB is responsible for processing the AgrD precursor, cyclizing it and secreting it from the bacterium.

Previous work of others including our group [17, 56] has enabled the identification and quantification of the auto-inducing peptide that is regulated by and also regulates the quorum sensing system in MRSA [16, 17] . Recently, we developed a mass-spectrometric method that enabled the simultaneous detection of multiple metabolites produced by MRSA [57]. Building off of this previous work, the goal of this project was to use identify features in mass spectrometry datasets associated with inhibition of the MRSA *agr* quorum sensing system. We sought to achieve this goal

using untargeted metabolomics and biochemometrics [6, 46, 48] analysis. A key element in conducting these experiments is the calculation of a multivariate statistical parameter called the "selectivity ratio" which is a quantitative measure of the extent to which any given feature in the metabolomics dataset correlates with the observed activity [46, 58-62].

Materials and Methods

Bacterial culture

A previously described method was used to evaluate the influence of inhibitors on MRSA metabolite production, with a slight modification [26]. Briefly a modified quorum sensing inhibitory assay [40] was used to allow for successful evaluation of metabolites influenced by the *agr* regulatory system. All bacteria strains used for this experiment were provided by Dr. Alexander R. Horswill. The clinically relevant strain of MRSA (LAC USA300) were cultured in a clear lid, medical grade, gamma sterilized polystyrene petri dish (Fisher Scientific) on approximately 10 mL of a mixture of solid trypticase soy broth (Sigma Aldrich) at 31 $g \times L^{-1}$ with microbiological grade agar (Fisher Scientific) at 15 $g \times L^{-1}$, in accordance with the ATCC guidelines. Plates were cultured in a Stuart microtiter Shaker Incubator (SI505). The bacteria were incubated at 37 ˚C and shaken at 250 rpm, overnight. The bacteria cultured petri dishes were visually inspected for consistent bacterial colonies before culturing. A single colony of each strain of bacteria was cultured in approximately 5 mL of TSB and incubated at 37 ˚C and shaken at 200 rpm in a New Brunswick Scientific shaker/incubator series I-26 for at least 18 to 24 hr. After incubation the culture broth was diluted 1:100 and cultured with shaking at

200 rpm at 37 ˚C for time period in between 2 hr and 4hr to allow a proper optical density reading using 600 nm wavelength (OD_{600}) in the range of 0.08 and 0.1. A 96-well tissue culture treated flat bottom plate (Corning Incorporated) was inoculated with 245 µL of diluted bacteria (200 µL TSB with addition of 45 µL of inoculated bacteria) and 5 µL of inhibitor, antagonist, or control in each well. The inhibitors included ambuic acid (Adipogen Life Sciences), a known signal-biosynthesis inhibitor of the *agr* regulatory system [40] and the potent antimicrobial chloramphenicol (Sigma Aldrich) [63-65]. These inhibitors were prepared at assay concentrations of 0.00µM to 100 µM, 0.00 µM to 300 µM, and 0.000 µM to 10 µM, respectively. Concentrated stock solutions of each were prepared in 100% microbiological grade dimethyl sulfoxide (DMSO) (Fisher-Scientific). Vehicle control consisted of 2% DMSO. Assays were performed in triplicate for each treatment and control. The plates were incubated at 37 ˚C and shaken at 1000 rpm in the previously mentioned Stuart shaker incubator. The OD_{600} was measured in 1 hr intervals using a Synergy H1 Plate Reader until the measurements reached 2.0 at which point, the experiment was considered complete. The total incubation time was approximately 4-6 hr. At completion of incubation, the culture broth containing bacteria was transferred to a clear, sterile 96-well, 0.22 µm hydrophilic plate with low protein binding durapore membrane (MultiScreen®) and filtered under vacuum. The spent media were then analyzed by UPLC-MS/MS.

UPLC-MS analysis of N-acetyl-L-histidine

We recently published a method for understanding *agr* regulatory metabolite production over time. That study yielded the optimized UPLC-MS analysis parameters used here [57]. This same method was employed for all metabolomics studies with the slight modification that the divert valve was turned off to enable detection of the early-eluting metabolite N-acetyl-L-histidine.

To confirm the identity of the N-acetyl-L-histidine, a standard of this compound (Sigma-Aldrich) was purchased and prepared in methanol and analyzed in parallel with MRSA spent media using the same UPLC-MS conditions [57] at a concentration of 10 $\mu g \times mL^{-1}$. Retention time, fragmentation pattern, accurate mass, and isotope pattern were compared between the standard and that of the putative N-acetyl-L-histidine ion in the MRSA spent media.

Results and Discussion

As demonstrated with the studies described in Chapter 2, treatment of MRSA with chloramphenicol strongly inhibited bacterial growth (**Figure 2.9A**), while ambuic acid treatment showed very little evidence growth inhibition (**Figure 2.9B**), but inhibited the production of MRSA metabolites known to be regulated by the *agr* system (**Figure 2.8**). Therefore, selectivity ratio analysis was employed to the untargeted metabolomics datasets for chloramphenicol (**Figure 3.1**) and ambuic acid-treated MRSA **(Figure 3.2**) to explore which metabolites correlated with growth, and of those that correlated with growth, which metabolites were regulated by quorum sensing system.

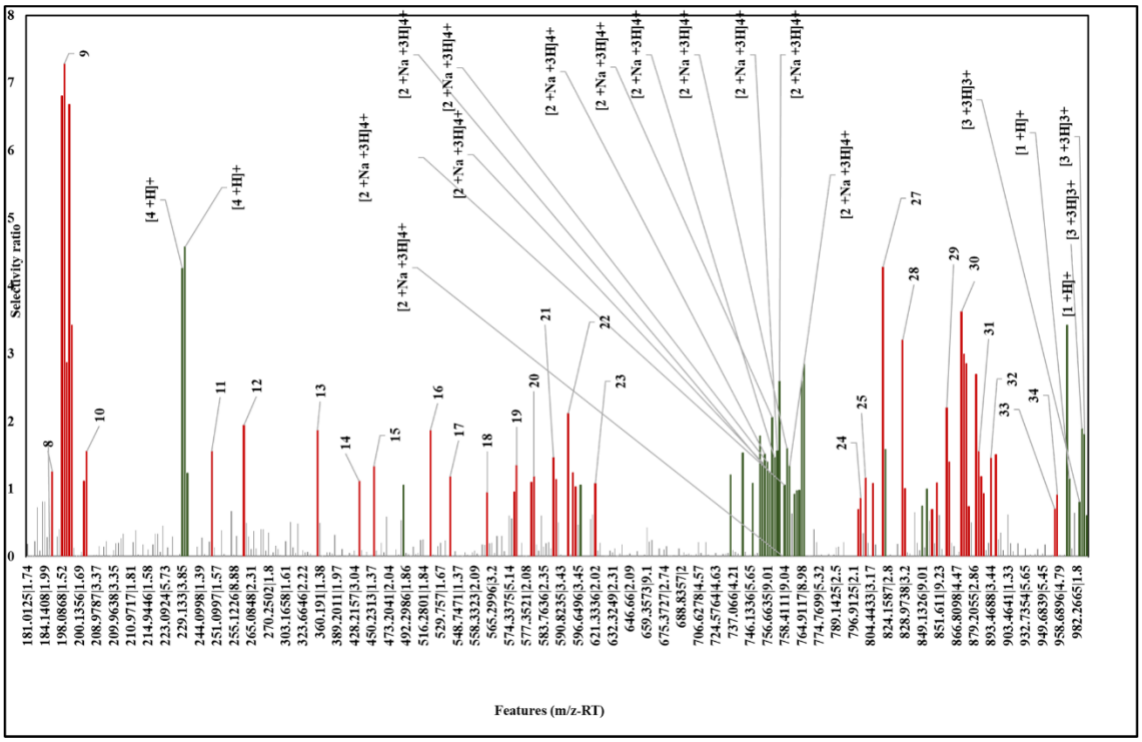

Figure 3.1. Selectivity ratio plot obtained for metabolomics analysis of MRSA (strain AH1263) treated with chloramphenicol with OD600 concentration as the dependent variable. The data was filtered to include 107 features, of which we were able to positively correlate 34 known and unknown metabolites with a SR > 1.0. Many of the detected features were isotopes, adducts, multiply charged ions, or in-source fragments of the know metabolites (**Table 2.1, Figure 3.1**). Several unknown metabolites were also determined to correlate with growth of MRSA based on the data shown in **Figure 3.1**, and these are shown in **Table 3.1** along with their charge state, if applicable, and adducts.

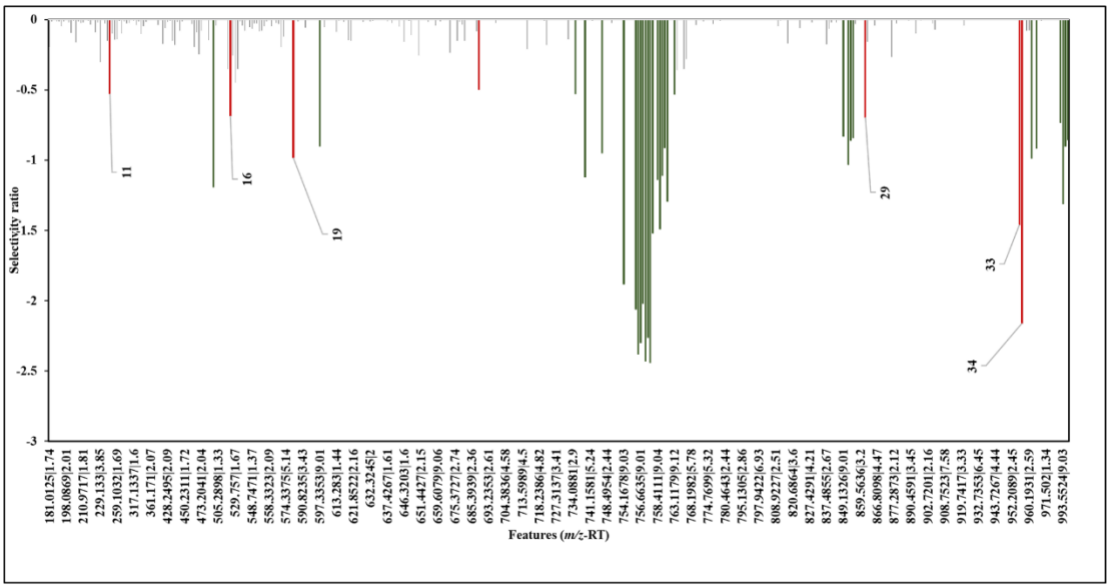

Figure 3.2. Selectivity ratio plot obtained for metabolomics analysis of MRSA (strain AH1263) treated with ambuic acid with ambuic acid concentration as the dependent variable. A total of 887 features were obtained in the dataset, with 36 features having a selectivity ratio of < -0.5. The numbers for known metabolites correspond to **Table 2.1** and the numbers for unidentified analytes correspond to **Table 3.1**, and these are shown in **Table 3.1** along with their charge state, if applicable.

Table 3.1. Features chosen based on selectivity ratio analysis of the data obtained by treatment of MRSA with chloramphenicol (Figure 3.1) or ambuic acid (Figure 3.2).

ID NUMBER	FEATURE (*M/Z*|*RT*)	CHARGE STATE	*AGR* REGULATED ?	Name (MOLECULAR FORMULA)
1	961.37789|3.26	+1	Yes	AIP-I ($C_{43}H_{61}N_9O_{12}S_2$)
2	745.4135|9.01	+4	Yes	δ-toxin ($C_{136}H_{225}N_{33}O_{39}S_1$)
3	752.4135|9.03	+4	Yes	formlyated δ-toxin ($C_{137}H_{225}N_{33}O_{41}S_1$)
4	245.1275|3.24	+1	No	Aureusimine A ($C_{14}H_{16}N_2O_3$)
5	229.1332|3.13	+1	No	Aureusimine B ($C_{14}N_{16}N_2O$)
6	769.4640|9.14	+3	Yes	PSMα-2 ($C_{110}H_{185}N25O_{27}S_1$)

7	586.4134|9.32	+3	Yes	PSMα-3 ($C_{110}H_{190}N26O30S_1$)
8	189.1261|1.67		No	--
9	198.0868|1.53	+1	No	*N*-acteyl-L-histidine ($C_8H_{11}N_3O_3$)
10	208.0964|1.43		No	--
11	247.1436|2.21	+5	Yes	
12	259.1032|1.69		No	--
13	360.1909|1.74		No	--
14	429.3060|1.32		No	--
15	451.7333|1.33		No	--
16	519.2691|1.66	+2	Yes	
17	542.3894|2.48		No	--
18	562.8196|4.40		No	--
19	575.9659|2.98	+2	Yes	In progress
20	581.6607|3.44	+3	No	--
21	588.6536|3.44	+3	No	--
22	594.3098|3.45	+3	No	--
23	621.3336|2.02	+1	No	--
24	797.6908|7.46	+4	No	--
25	798.1927|6.19	+4	No	--
26	804.6061|2.86	+4	No	--
27	815.4288|2.11	+1(?)	No	--
28	828.4717|3.21	+2	No	--
29	863.4461|2.98	+2	Yes	--
30	871.4870|3.44	+2	No	--
31	882.4778|3.44	+2	No	--
32	893.4688|3.44	+2	No	--
33	957.5439|3.14	+2	Yes	Peptide In progress
34	958.0460|3.13	+2	Yes	Peptide In progress

Of the unknown metabolites shown in **Table 3.1**, we were particularly interested in those that regulated by the quorum sensing system. To identify which metabolites were *agr* quorum sensing system regulated, a similar selectivity ratio plot was constructed of the ambuic acid treated data set (**Figure 3.2**). For this selectivity ratio plot, ambuic acid

concentration was used as the dependent variable. Features with strongly negative selectivity ratio values were the features of interest, as these were the features that decreased in abundance with increasing concentration of ambuic acid added to the MRSA cultures. Upon filtering, 34 features were identified with selectivity ratios below the empirically determined cut-off of -0.50 and labeled as "*agr* regulated" in **Table 3.1**. To confirm the trends predicted by the selectivity ratio analysis (**Figures 3.1** and **3.2**), we plotted dose-response curves for all of the ions listed in **Table 3.1.** For these curves, we plotted abundance (peak area of the relevant selected ion trace) versus concentration of either ambuic acid or chloramphenicol in the culture medium. Our prediction was that metabolites regulated by the *agr* system would display a decrease in peak area in response to both treatment with ambuic acid and treatment with chloramphenicol. An example of this is shown for two *agr*-regulated metabolites in **Figure 3.3 A-D**, at *m/z* 958.0460 and 863.4461. Metabolites associated with MRSA growth but *not* regulated by the *agr* system would show a decrease in peak area only in response to treatment with chloramphenicol. An example of this is shown for the metabolite detected at *m/z* 198.0868 (**Figure 3.3 E, F**), which was ultimately identified as N-acetyl-L-histidine, as described in the next section.

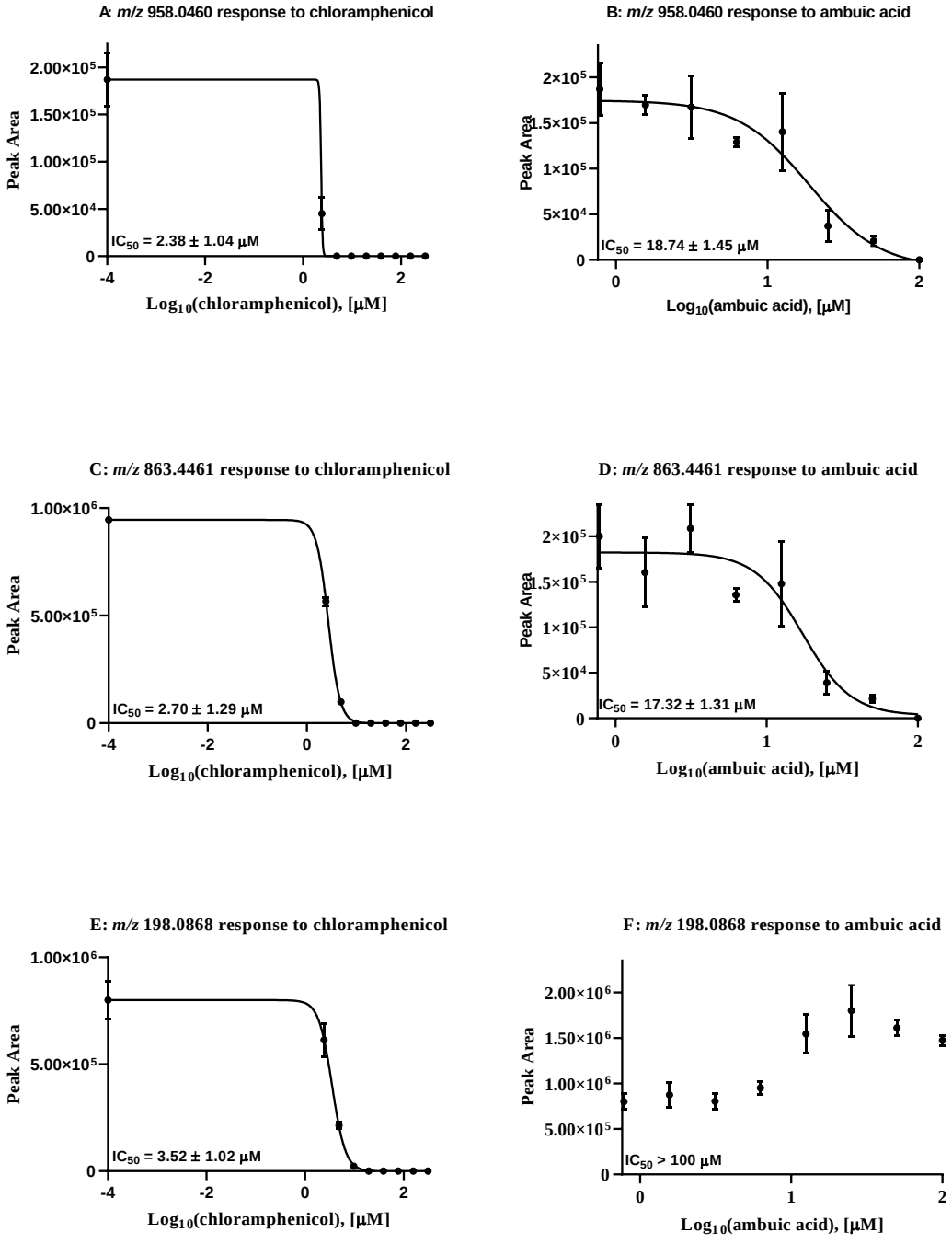

Figure 3.3. Dose-response curves of unknowns. N-acetyl-L-histidine was is represented by (E and F). This supports our prediction that N-acteyl-L-histidine is not controlled by the quorum sensing system.

Identification of Unknowns

As shown in **Table 3.1**, we assigned charge state of each of the unknown features based on spacing between isotopes. Due to the low abundance of these unknowns, we were unable to obtain a molecular formula for the high mass metabolites shown in **Table 3.1**. However, molecular formula could be predicted for accurate mass of one of the growth-associated metabolites, which was detected as a singly charged ion at *m/z* 198.0868. Based on published literature [66], we hypothesized that the identity of this metabolite was N-acetyl-L-histidine, a known metabolite of *Staphylococcus aureus* with molecular formula of $C_8H_{11}N_3O_3$. An authentic standard for N-acetyl-L-histidine was obtained, and the identity of the unknown metabolite was confirmed by comparing retention time, accurate mass, and MS/MS spectra to that of the standard [67] (**Figures 3.4 and 3.5)**.

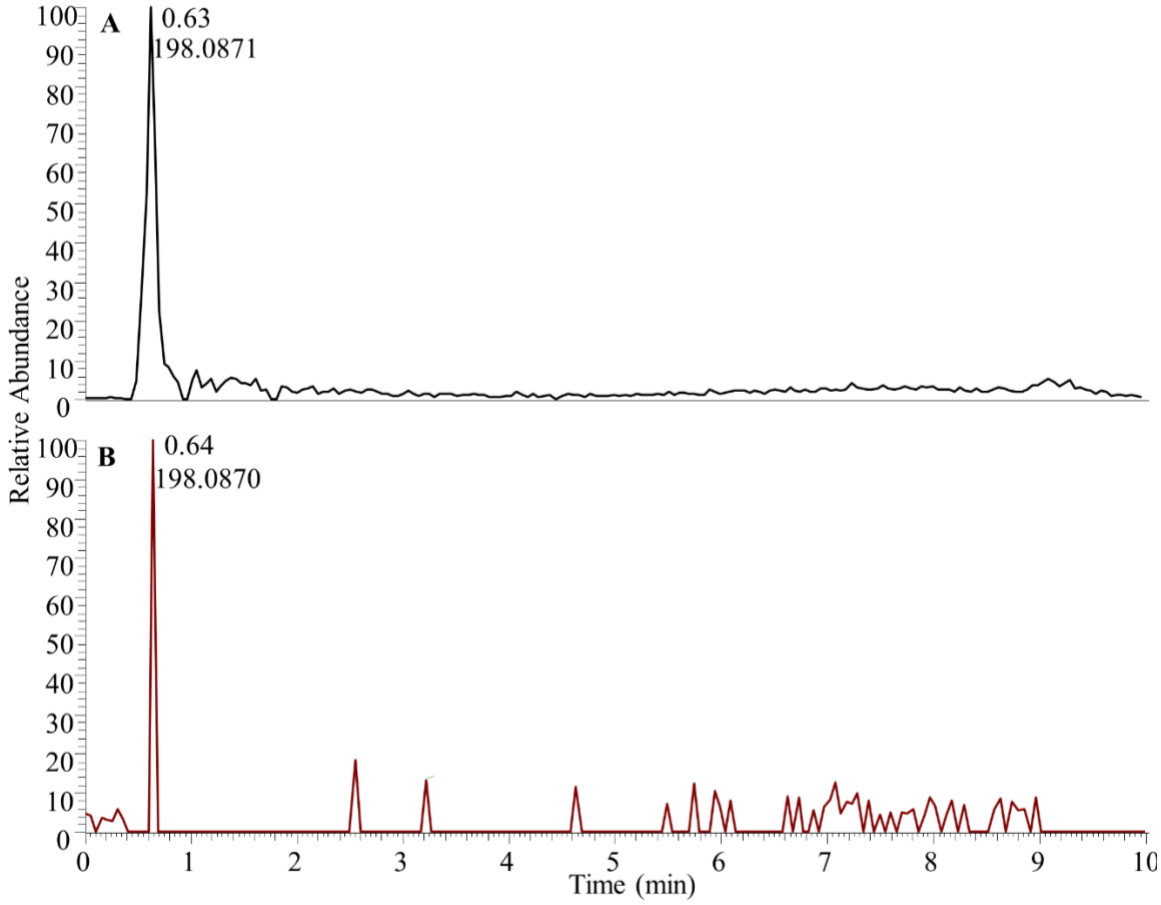

Figure 3.4. Selected ion chromatograms for *m/z* 198.0868 (calculated monoisotopic mass for $[M+H]^+$ N-acetyl-L-histidine with 5 ppm mass tolerance). (A) represents analysis of an N-acetyl-L-histidine standard at a concentration of 10 µg/mL while B represents analysis of the culture broth of MRSA (AH1263).

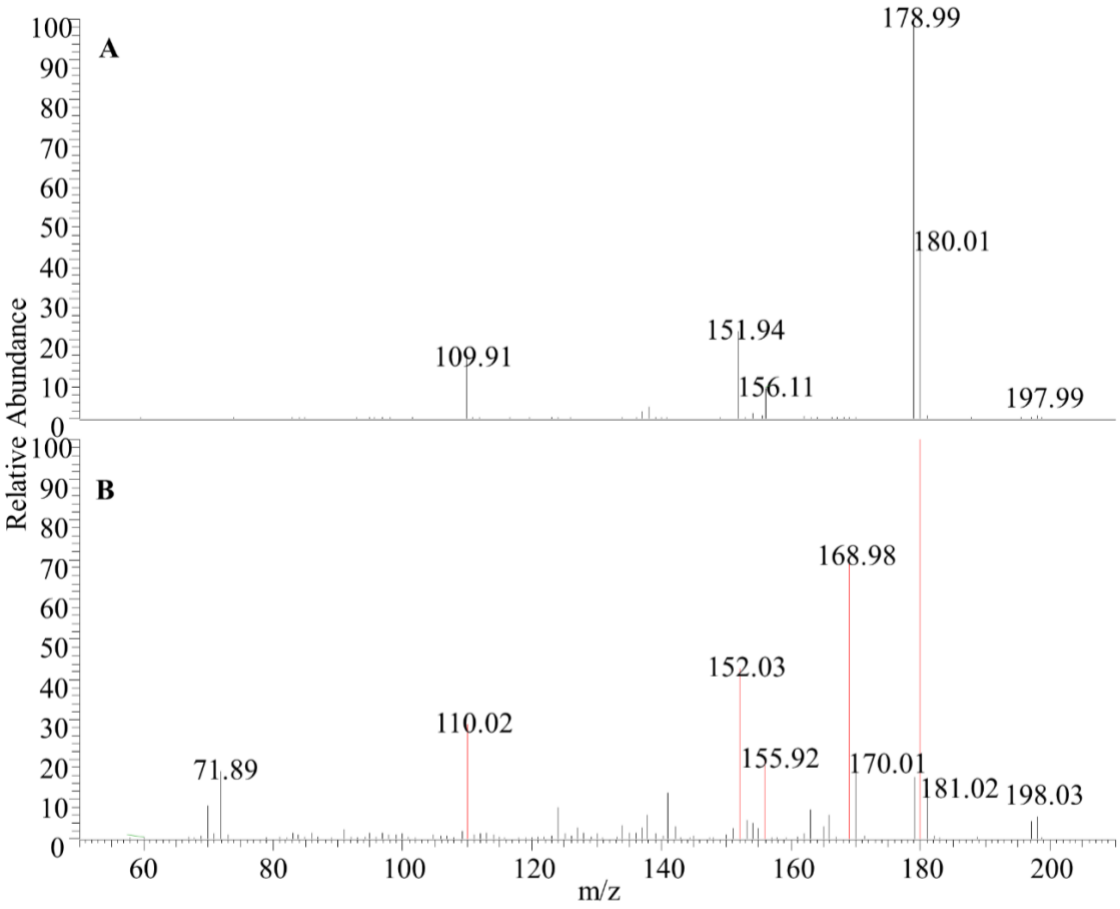

Figure 3.5. MS-MS data obtained by collision induced dissociation (CID) of the precursor ion at *m/z* 198.0868 (calculated monoisotopic mass for $[M+H]^+$ N-acetyl-L-histidine). A 5 ppm mass tolerance for (A) N-acetyl-L-histidine standard at a concentration of 10 µg/mL and (B) analysis of the culture broth of MRSA (AH1263).

Conclusion and Future Directions

With these studies, we confirmed the presence of multiple unknown metabolites in MRSA cultures. Several of the unknown metabolites were associated with MRSA growth but not *agr* regulated, and the identity of these was confirmed to be N-acetyl-L-histidine by comparison with an authentic standard. N-acetyl-L-histidine production

could be used to monitor MRSA growth, as described in Chapter 2 for our studies with aureusimines.

The metabolites regulated by the *agr* system are of particular interest, as they might constitute new virulence factors of MRSA. It is also possible, however, that these metabolites could be degraded products of other known *agr* outputs. The identities and biological function of the *agr* regulated metabolites are the subject of ongoing experiments. For these studies, we are scaling up MRSA cultures with the goal of isolating material for NMR analysis or producing sufficient MS signal to enable interpretation of MS-MS fragmentation spectra.

CHAPTER IV

IDENTIFICATION AND QUANTIFICATION OF ANTIMICROBIAL COMPOUNDS FROM RUMEX CRISPUS WITH UNTARGETED METABOLOMICS

This chapter is under preparation for submission to *Planta Medica.* Chantal V. Pelzer, Joëlle Houriet, Daniel A. Todd, William J. Crandall, Nadja B. Cech and Derick D. Jones Jr.[1*]

Derick D. Jones, Jr. supervised the work conducted as part of this project, helped with the design and execution of experiments and interpretation of data, wrote the first draft of the manuscript (with assistance from Chantal V. Pelzer) and provided mentorship to Chantal V. Pelzer. Chantal V. Pelzer conducted the experiments (with assistance from Derick D. Jones, Jr.), conducted literature reviews, and assisted with manuscript preparation. Daniel A. Todd assisted in designing MS methods and in collection and interpretation of MS data. William J. Crandall and Joëlle Houriet assisted with data analysis and preparation of figures. Nadja B. Cech acquired research funding and helped to draft and edit the manuscript and interpret the data.

Introduction

Botanicals are a major source of medicinally relevant compounds used to combat a multitude of diseases. Plant-based medicines are a major form of healthcare for an estimated 80% of the world's population [68]. Existing literature has reported the biological significance and activity [6] of many chemical constituents present in botanicals. These include alkaloids [1], saponins [69], terpenoids [70], and polyphenols [4]), to name a few. As a result of the differing biological activity but similar chemical structures and properties (in some cases), separation and purification of compounds have

presented distinct analytical challenges*Rumex crispu*s is a member of the Polygonaceae family originally native to Europe and Asia but now seen in many countries [71]. It is a common weed of agriculture found especially in grassy areas, waste ground, roadsides, and near sand dunes [71]. The genus contains roughly 200 species [71]. *Rumex crispu*s has extensive history in being used as an herbal remedy for its cleansing properties, and its holistic effect with people suffering from chronic skin problems in traditional medicine in many cultures [72]. The root of this plant has been traditionally by being mashed up or as a dried powder to treat sores, ulcers, wounds, and various other skin disorders [73].

Rumex crispus is rich in a chemical class of compounds known as anthraquinones, which are reported to possess antimicrobial activity [74]. Of the anthraquinones from *R. crispus*, emodin is one of the most widely studied, and it is found in the root and bark of this and other plants, including various Chinese herbs. The compound is often physically described as an orange needle or powder derived from alcohol or by sublimation [71]. Herein, we sought to determine where emodin is responsible for the purported effectiveness of *R. crispus* as an antimicrobial against methicillin resistant *Staphylococcus aureus*. We predicted based on the complexity of *R. crispus* root extracts that other constituents might also contribute to the activity of this botanical

Materials and Methods

General experimental procedures

UPLC-MS analysis was completed in negative mode using a Q-Exactive Plus mass spectrometer (Thermo Fisher Scientific) connected to an Acquity UPLC system

(Waters Corporation). When collecting UPLC-MS data, 3 μL of 1 mg × mL^{-1} samples suspended in MeOH were injected into the column. Using a flow rate of 0.3 mL × min^{-1}, samples eluted from the column (BEH C18 1.7 μm, 2.1 × 50 mm, Waters Corporation) using the following gradient with solvent A consisting of water with 0.1% formic acid and solvent B consisting of acetonitrile with 0.1% formic acid: 90:10 (A:B) from 0-0.5 min, increasing to 0:100 (A:B) from 0.5-8.0 min. The gradient was isocratically held at 100% B for 0.5 min, before returning to starting conditions over 0.5 min and held from 9.0-10.0 min. Mass analysis was completed in both positive and negative ionization modes over a scan range of 150-1500 with the following settings: capillary voltage at -21.00 V, capillary temperature at 256.25 °C, tube lens offset at -95.00 V, spray voltage at 3.50 kV, sheath gas flow at 47.50, and auxiliary gas flow at 11.25.

Flash chromatographic separations were completed using A CombiFlash RF system (Teledyne-Isco) was used for flash chromatographic separation and this separation was examined using a PDA detector and an evaporative light scattering detector (ELSD).

Plant material

Fresh roots of *Rumex crispus* were collected on June 20, 2019 from the University of North Carolina at Greensboro Garden in Greensboro, North Carolina (N 36.07°, W 79.81°). A voucher specimen of *Rumex crispus* roots was deposited at the herbarium of the University of North Carolina at Chapel Hill (NCU671166).

Extraction

Fresh *Rumex crispus* roots were dried in a single wall transite oven (Blue M Electric Company) at 37 °C for 24 hours. The resulting dry mass (64.00 g) was ground using a Wiley Mill Standard Model No. 3 (Arthur Thomas Company) and submerged in methanol (MeOH) (Fisher Scientific, ACS grade) at 160 $g \times L^{-1}$ for 24 hours. The resulting MeOH was drained from plant material and dried in a round bottom flask (Fisher) using a rotovap (G3 Heidolph, Heidolph Instruments). Plant material was resubmerged for 24 hours with the MeOH previously extracted from the rotaovap. This process was repeated twice more (4 total). During the last extraction, the MeOH was drained as before without drying down. Doubly deionized water (H_2O) was added to MeOH (9:1 MeOH:H_2O) and then sonicated to dissolve sum of the three extractions of the plant material in the same round bottom flask. The mixture was transferred into a separatory funnel for partitioning. The MeOH/H_2O mixture was partitioned with hexane (1:1 MeOH/H_2O: Hexane). The hexane was measured using a graduated cylinder. Hexane was transferred to the round bottom flask, gently swirled and slowly poured into the separatory funnel (repeated 3 times to include as much of the organic compounds from the round bottom flask as possible). The aqueous MeOH layer was partitioned further with ACS grade ethyl acetate (EtOAc) (Fisherscientific) empirically (4:1 EtOAc/MeOH/H_2O). To remove hydrosoluble tannins, the EtOAc layer was washed with a 1% sodium chloride (NaCl) solution. The resulting EtOAc extract was dried under nitrogen, yielding 2470 mg dried extract, before chromatographic separation.

Chromatographic separation

The first-stage separations of the EtOAc extract (2470 mg) were conducted using normal-stage flash chromatography on a 40 g silica gel column.[45] The ELSD was set to 55 $°C$ and pressure of 1.5 bar. The nitrogen gauge was set at 20 psi. A 40 mL × min^{-1} flow rate was used and a total column volume (CV) of 89.2 over a hexane/$CHCl_3$/MeOH gradient. The gradient consisted of ACS grade chloroform ($CHCl_3$) (Fisher Scientific) as solvent A1, methanol as solvent B1, and hexane as solvent B2. ISCO runs a dual solvent system and changes solvent within the duration of the run. At the beginning of the run, B2 was held isocratically at 100% for 5 CVs. The gradient (A1:B2) began at 5 CVs as B2 decreased to 0% for 22 CVs. B2 was switched to B1 for 5 CVs. The gradient (A1:B1) increased to 0:100 for 32 CVs and B1 was held at 100 % for the last 25.2 CVs.

Antimicrobial assay

To evaluate antimicrobial activity, broth dilution assays were conducted by assessing growth inhibition of a clinically relevant strain of methicillin-resistant *S. aureus* (MRSA USA300 LAC strain AH1263) using Clinical Laboratory Standards Institutes (CLSI) methods [75]. This strain was obtained from Dr. Alexander Horswill at the University of Colorado Anschutz Medical Campus. Cultures were grown from a single colony isolate of MRSA in Müeller-Hinton broth (MHB) and diluted to 1.0 $\times 10^5$ CFU × mL^{-1} based on absorbance at 600 nm (OD_{600}).

Rumex crispus roots extract and fractions were screened in triplicate at final concentrations of 10 and 100 μg × mL^{-1}. Samples were dissolved in microbiological grade dimethyl sulfoxide (DMSO) (Fisher Scientific) and diluted with Müller hinton

broth (MHB) (Sigm-Aldrich) to prepare final concentrations in broth with less than 2% DMSO. The known antibiotic chloramphenicol (98% purity, Sigma-Aldrich) was used as a positive control at the same concentrations as tested extracts and fractions. The vehicle was 2% DMSO in MHB. Blank wells consisted of samples at concentrations of 10 and 100 $\mu g \times mL^{-1}$ without bacteria to use as a comparison for bacterial growth. Bacteria wells were inoculated and incubated for 24 hours at 37 °C. OD_{600} was evaluated after incubation and used to calculate the percent growth inhibition for biochemometric analysis (explained in detail in the section describing *untargeted metabolomics analysis*).

Minimal inhibitory concentrations (MICs) were calculated for emodin (analytical standard, ≥ 97% purity, Sigma-Aldrich) and chloramphenicol (positive control, 98% purity, Sigma-Aldrich). The MIC is representative of the concentration at which either the control or the pure standard has completely inhibited the growth of bacteria. The inhibitory concentration at which bacterial growth is inhibited by 50 %, known as the IC_{50} or the EC_{50} were also calculated in order to properly predict activity of emodin based on the concentration of emodin in each sample. These values were determined using graphpad prism software (version 8.4.3) and can be further visualized in **Figure 4.3**. Emodin and chloramphenicol were added to 96-well plates in triplicate at concentrations ranging from 0-200 $\mu g \times mL^{-1}$ in MHB. Broth containing 2% DMSO was used as the vehicle control. The concentration of DMSO was set at a fixed value of 2% for all wells. After a 24-hour incubation at 37 °C, OD_{600} values were measured. The MIC was defined as the concentration at where no statistically significant difference between the blank wells (containing sample and broth but no bacteria) and the treated sample was observed.

Quantification of emodin and prediction of antimicrobial activity

A calibration curve of emodin was constructed to quantify the amount of emodin in the extract and the subfractions of the extract. Emodin standards were prepared at a range of 1.00×10^{-3} to 1.00×10^{2} µg × mL^{-1} in optima grade methanol (Fisher-Scientific and analyzed by UPLC-HRMS as described below. Emodin concentration was determined by linear regression analysis of this calibration curve (*Equation 4.1*) where Y is the $\log_{10}$ (peak area of the ion at *m/z* 269.0455 for emodin in extract and fractions), m (0.5723) is the slope of the calibration curve, X is the $\log_{10}$(concentration of emodin, µg × mL^{-1}), and b (8.3240) is the y-intercept of the calibration curve.

$Y = mX + b$ *Equation 4.1*

The predicted antimicrobial activity of emodin (*Equation 4.2*) was calculated based on its concentration in each extract and fraction and the dose-response relationship for growth inhibition of *Staphylococcus aureus* (Figure 1B). This approach is similar to that employed by Caesar *et. al*. to predict antimicrobial activity of botanical extracts [76]. Where Y is the predicted biological response emodin will have at a given concentration, min is the bottom of the dose-response curve (-0.2205), max is the top of the curve (0.9280), IC_{50} is the value for the point midway between the max and min also referred to as the half-maximal inhibitory concentration. The hillslope is a numerical value that characterizes the steepness of the slope at the midpoint (-0.603). Finally, x is the concentration of emodin in each extract and fraction (calculated in *Equation 4.1*).

$$Y = \min + \frac{\max - min}{1+(\frac{x}{IC_{50}})^{-hillslope}} \quad \textit{Equation 4.2}$$

Untargeted metabolomics analysis

UPLC-HRMS data were collected in negative mode and analyzed, aligned, and filtered utilizing MZmine 2.21.2 (http://mzmine.sourceforge.net/) [45] Raw mass spectral data files from first-stage fractions were uploaded for peak picking into MZmine. Chromatograms were constructed for all *m/z* values lasting from 1 to 10 minutes. The peak detection parameters were set as follows: noise level (absolute value) at 1×10^6, signal to noise threshold at 5, coefficient to area threshold at 10, minimum peak duration at 0 to 3 minutes, retention time wavelet range at 0 to 0.05, retention time tolerance at 0.5 min., and *m/z* intensity tolerance at 20%. Peaks were aligned if their masses were within 5 ppm from one another. Peak list filtering and retention time alignment were completed to produce an aligned peak list. The resulting data matrix, consisting of *m/z*, retention time, and peak area, was exported as a csv file to Excel (Microsoft). Filtered chemical data was merged with MRSA inhibition data from samples at tested at 100 $\mu g \times mL^{-1}$ to form the final data set for ready to be imported into software that can carry out bioinformatic approaches [77].

Selectivity ratios were calculated using Sirius version 10.0 statistical software (Pattern Recognition Systems) [77]. Before analysis, data were adjusted using a transformation to normalize noise [78]. An internally cross-validated PLS model was then produced using 100 iterations and a significance level of 0.05. Statistical algorithms

internal to the Sirius software utilized model predictions to produce selectivity ratios identifying putative antimicrobial constituents.

Results and Discussion

Dose-response analysis of emodin and chloramphenicol against MRSA

Chloramphenicol and emodin served as controls in this study, and the minimum inhibitory concentration of these compounds was evaluated for the purpose of establishing a baseline for comparison with this study and with published data [79]. The concentration of the known antimicrobial ranged from 0 to 200 $\mu g \times mL^{-1}$. The MIC for chloramphenicol was at 12.5 $\mu g \times mL^{-1}$ (**Figure 4.1 A**) and the MIC for purified emodin was 200 $\mu g \times mL^{-1}$ (**Figure 4.1 B**). Due to limited solubility, 200 $\mu g \times mL^{-1}$ was the highest emodin concentration tested, but growth inhibition was >95% at this concentration, qualifying it as the MIC.

A. Chloramphenicol Dose Response Curve

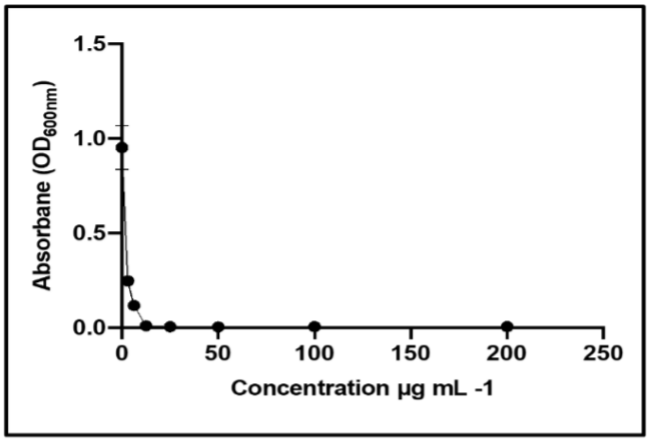

B. Emodin Dose Response Curve

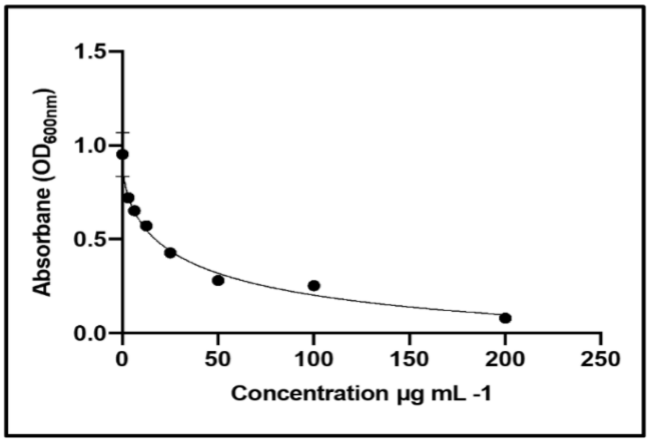

Figure 4.1. Antimicrobial activity of chloramphenicol. (A) with minimum inhibitory concentration **12.5 µg × mL $^{-1}$** and emodin (B) with minimum inhibitory concentration greater than **200 µg × mL $^{-1}$** against MRSA LAC USA300. Both chloramphenicol and emodin were tested at concentrations ranging from **0 to 200 µg × mL $^{-1}$** in biological triplicates. Samples were incubated for 24 hours and MRSA growth was measured by turbidity (OD_{600}). The standard deviation was calculated and is indicated by the error bars. For the purpose of this study MIC was defined as the concentration at which bacterial growth was inhibited by ≥ 90 %.

Antimicrobial activity of R. crispus extracts and fractions

Antimicrobial activity of a series of fractions from a complex *R. crispus* extract at two concentrations (10 and 100 µg × mL^{-1}) against MRSA is shown in **Figure 4.2A**.

Fraction 3 demonstrated the most potent antimicrobial activity against methicillin-resistant *Staphylococcus aureus* (MRSA, strain USA300 LAC) [41]. Fractions 4-8 also inhibited MRSA growth (**Figure 4.2 A**) in a dose dependent fashion, but with less potency.

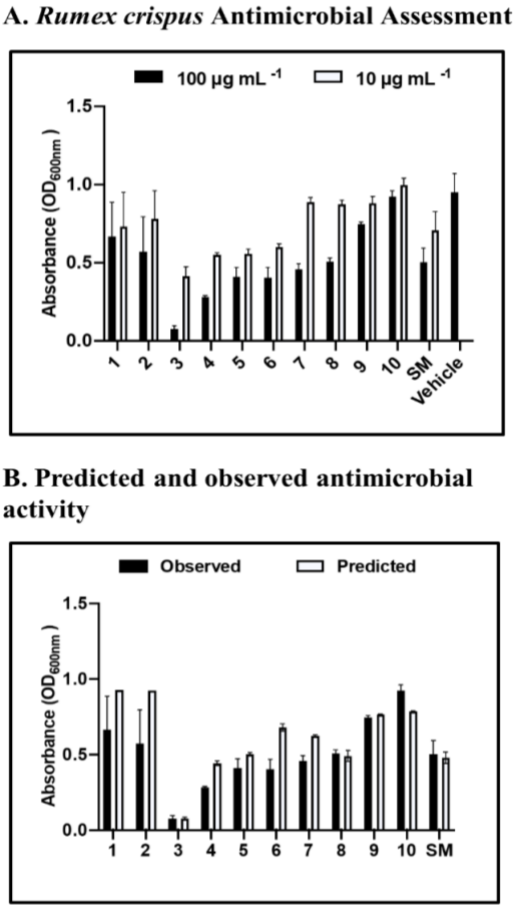

Figure 4.2. Antimicrobial activity of *Rumex crispus* roots fractions 1-10 and extract at concentrations 100 µg × mL $^{-1}$ and 10 µg × mL $^{-1}$ (expressed as mass of extract or fraction per assay well volume) with DMSO as vehicle. Fractions **3-7** are the most active against MRSA LAC USA300 with percent inhibition > 50%. Comparison of predicted and observed antimicrobial activity of *R. crispus* fractions **1-10** and starting material (SM) at an assay concentration of **100 µg × mL $^{-1}$** based on the content of emodin in each. Activity was evaluated against MRSA LAC USA300 **(A)**. Fraction 3 has

no significant difference in observed and predicted values, however; active fraction 4-7 have a greater observed than predicted activity **(B)**.

To determine whether the observed antimicrobial activity of the *R. crispus* fractions could be attributed to the known antimicrobial constituent emodin, UPLC-MS was used to identify and quantify this compound in the fractions (**Figure 4.2B**, **Figure 4.3**).

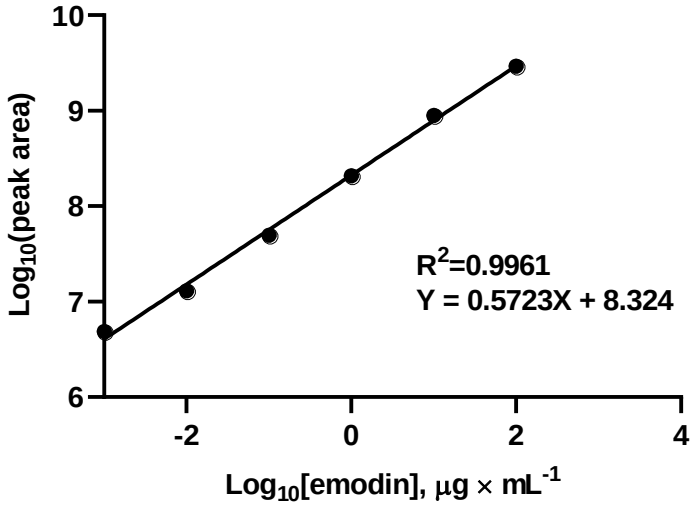

Figure 4.3. **Calibration curve of emodin was used to obtain the concentration of emodin in the *Rumex crispus* extract.** The x- and y-axis were both transformed to express values in the Log_{10}. The concentration range of emodin used to make the calibration curve was **1.00×10^{-3}** to **1.00×10^{2} µg × mL^{-1}**.

In parallel, the correct identification of emodin was confirmed by comparing the following qualities between the putative emodin in the *R. crispus* extract and purified emodin in negative polarity mode $[M-H]^-$ *(1)* accurate mass of 269.0457 ion *(2)* retention time. Excellent agreement was observed between the standard and the putative emodin in the *R. crispus* extract (**Figure 4.4**).

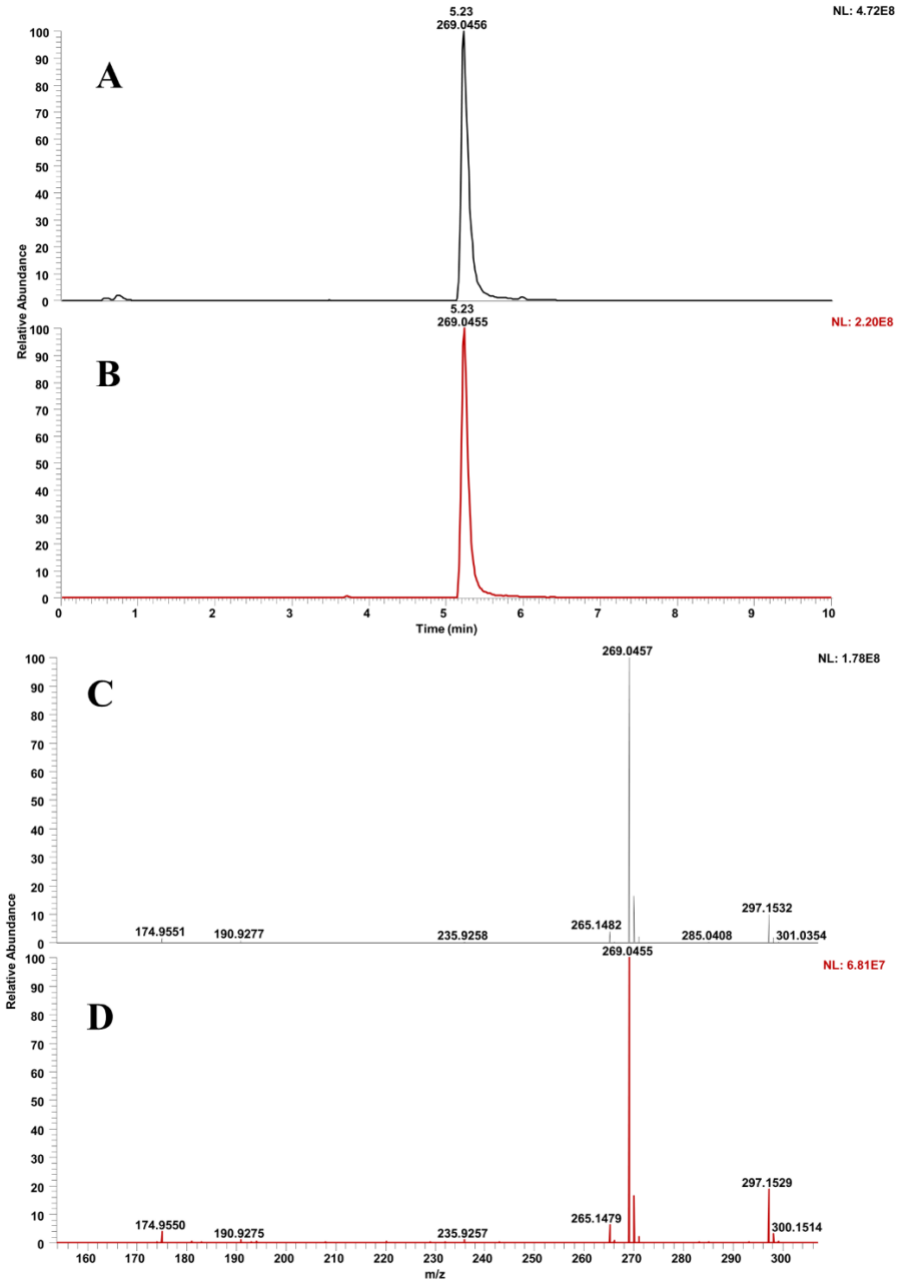

Figure 4.4. Comparison of the chromatographic data (A, B) and mass spectral data (C, D) for a an emodin standard (A and C) and the putative emodin ion in the *Rumex crispus* extract (B, D). Excellent agreement is observed in both retention time and accurate mass between the emodin standard and the ion that is assigned to emodin in the *R. crispus* extract.

Figure 4.2B shows calculated (predicted based on MIC and quantity of emodin in each fraction) and measured antimicrobial activity of the *R. crispus* extracts and fractions. The concentration of emodin in each fraction was calculated using linear regression based on the calibration curve shown in **Figure 4.4** from *Equation 4.1*. The predicted activity shown in **Figure 4.2B** was calculated using *Equation 4.2*. While fractions 1-3 showed close alignment between predicted and observed activity, fractions 4-7 displayed higher activity than that which was predicted based on the measured emodin content (**Figure 4.2B**). These results demonstrate that the activity of fractions 4-7 must be partially attributable to compounds other than emodin.

Untargeted metabolomics to identify features associated with antimicrobial activity

Supervised analysis of metabolomics data was carried out using orthogonal partial least squares discriminant analysis (OPLS-DA). The purpose of this analysis was to determine which features detected in the *Rumex crispus* extract were most strongly associated with antimicrobial activity against MRSA, and to propose possible features (beyond emodin) that might be responsible for the antimicrobial activity of *R. crispus*. Bacterial growth as measured by the OD600 was used to guide our analysis, serving as the dependent variable. The independent variables were the features, each one representing a mass to charge, retention time pair (*m/z*-RT).

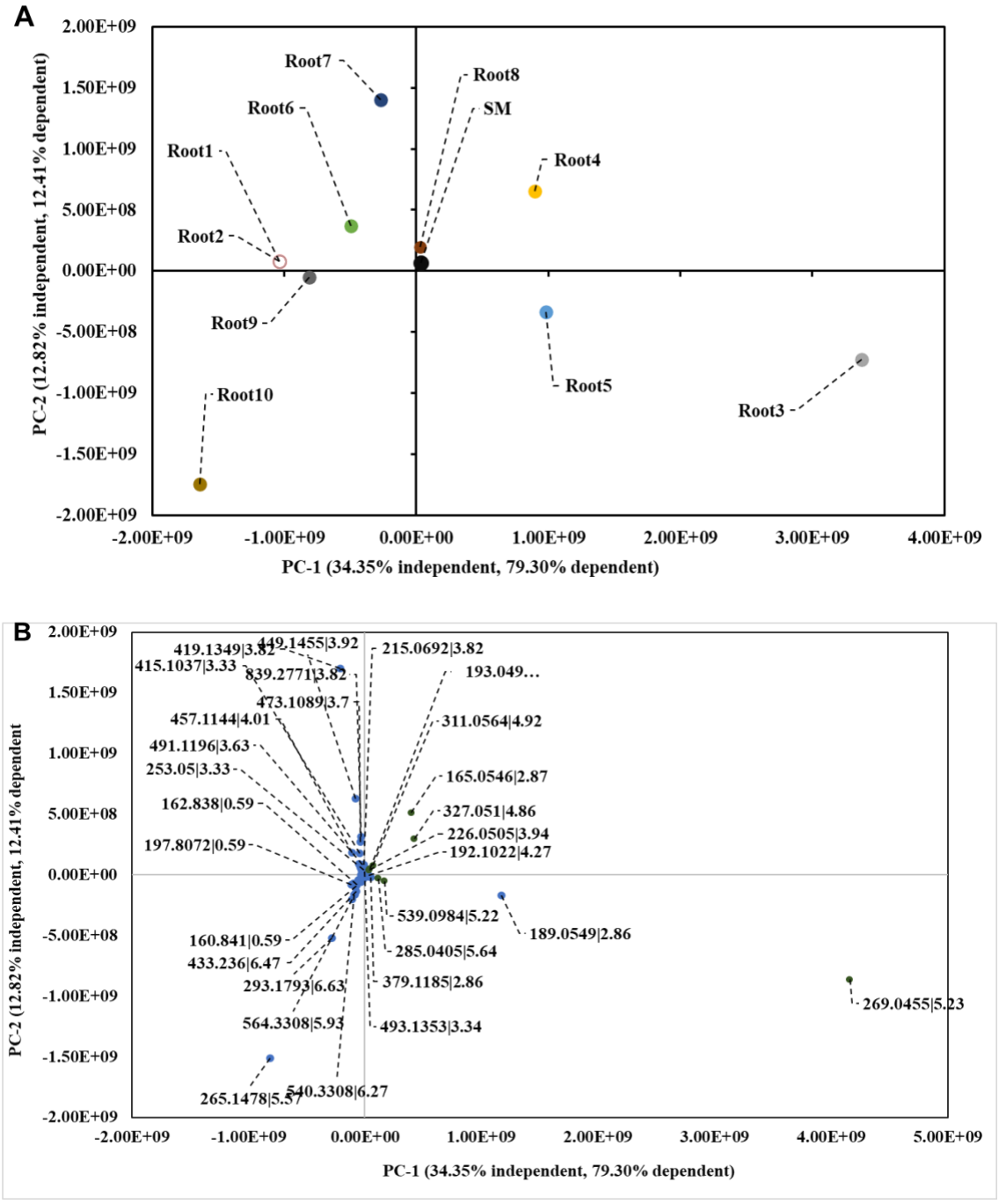

Figure 4.5. Orthogonal partial least squares discriminant analysis (OPLS-DA) scores plot (A) and loadings plot (B) of *R. crispus* fractions 1-10 and extract (SM). tested for antimicrobial activity against *Staphylococcus aureus* at **100 µg × mL $^{-1}$**. MRSA growth inhibition was measured in triplicate using OD600, the fractions, extract and pure compounds were analyzed from UPLC-HRMS (via Acquity UPLC and Q-Exactive

orbitrap mass spectrometer) in triplicate. An independent chemical analysis by LC-MS was conducted for each solution measured in the antimicrobial assay. Datapoints shown in green also demonstrated selectivity ratio values (SR) greater than 0.1 and are highlighted in **Figure 4.6**.

OPLS-DA was utilized to describe the variance between each sample (starting material and fractions) of *Rumex crispus*. The scores plot is a visual representation of how the fractions group according to their antimicrobial activity. The loadings plot depicts the features (*m/z*-RT pair), with their position in the plot demonstrating to what extent they explain the difference among sample.

A second way of displaying the correlation between biological activity and chemical composition is the selectivity ratio plot (**Figure 4.6**). Selectivity ratio analysis is used for this project as a ranking to determine which features of the *R. crispus* extract are associated with its antimicrobial activity. The selectivity ratio is the ratio of the explained variance to the unexplained variance in the dataset [77, 78, 80]. Features that are correlated with bioactivity will have strong positive selectivity ratios. For the data shown in **Figure 4.6**, emodin at *m/z* 269.0457, RT 5.23 min was positively correlated the most with MRSA growth inhibition by *Rumex crispus* fractions. Although emodin displays the highest positive correlation with increased bacterial growth inhibition, one of advantages of using the selectivity ratio analysis is the ability to detect and predict the activity of features detected at low levels [77, 80]. This analysis allowed us to identify more metabolites from *R. crispus* that correlated to the inhibition of MRSA growth (**Figure 4.6**). A selectivity ratio cut off of 0.10 was employed, which yielded a total of 10 features. Peaks 5 and 10 is emodin at *m/z* 269.0455 (ID5), and a dimer of emodin *m/z*

539.0435 (ID 10), respectively. The level confidence of the identity of the annotated compounds are based upon scoring system described in previous literature [81]. **Table 4.1** refers to these scores as the MSI level of confidence. The scores ranged between 1 and 4. Feature-ID 5 and 10 had a MS-I level of confidence score of 1. For features to have this score a standard (emodin, in this case) was used to confirm retention time and accurate mass. Features with a confidence level of 2 (Feature-ID 1 and 6) were annotated based on their level of similarity to mass spectral data from its identification of plants of the same species. Confidence level 3 features were annotated because these small molecules had previously been identified in plants of the same genus or family. Confidence level 4 are unknown features, for which it is possible to predict a molecular formula based on MS spectral data, isotope pattern score to the online databases, and the accurate monoisotopic mass matching that of the predicted molecular formula within a tolerance of ± 10. All annotations in Table 4.1 are putative; further experiments employing NMR and other spectroscopic techniques for structural elucidation would be needed to confirm identities of these species.

Table 4.1. Features identified as having selectivity ratios (Figure 4.6) ≥ 0.10 are shown along with MSI level of confidence [81] for assignment of structure.

ID	Features (*m/z*-RT)	Molecular formula	Compound name	Polarity	[ppm]	Isotope pattern score	MSI level of confidence [81]
1	165.0546|2.87	$C_9H_{10}O_3$	2',6'-Dihydroxy-4'-methyla	$[M-H]^-$	-6.6	98.8%	2

			cetophenone (syn. 2-acetylorcinol)				
2	191.034|2.96	$C_{10}H_8O_4$	Unknown feature	$[M-H]^-$	-5.0	98.6%	4
3	193.0497|3.08	$C_{10}H_{10}O_4$	5,7-Dihydroxy-1(3*H*)-isobenzofuranone; Di-Me ether (syn. 5,7-dimethoxyphtalide	$[M-H]^-$	-4.7	98.4%	3
4	226.0505|3.94	$C_{13}H_9NO_3$	Unknown feature	$[M-H]^-$	-2.0	97.0%	4
5	269.0455|5.23	$C_{15}H_{10}O_5$	emodin (1,3,8-Trihydroxy-6-methylanthraquinone)	$[M-H]^-$	-0.1	99.4%	1
6	285.0405|5.64	$C_{15}H_{10}O_6$	1,5,7-Trihydroxy-2-hydroxymethylanthraquinone	$[M-H]^-$	0.2	96.8%	2

7	311.0564|4.92	$C_{17}H_{12}O_6$	1,8-Dihydroxy-3-(hydroxymethyl)anthraquinone1'-Ac	$[M-H]^-$	1.0	96.6%	3
8	327.051|4.86	$C_{17}H_{12}O_7$	Unknown feature	$[M-H]^-$	0.0	98.8%	4
9	523.1397|6.68	$C_{31}H_{24}O_8$	Unknown feature (in DNP, dimer of emodin, from Marine source [82]	$[M-H]^-$	-0.2	90.7%	4
10	539.0984|5.22	$C_{30}H_{20}O_{10}$	emodin dimer	$[2M-H]^-$	0.1	90.4%	1

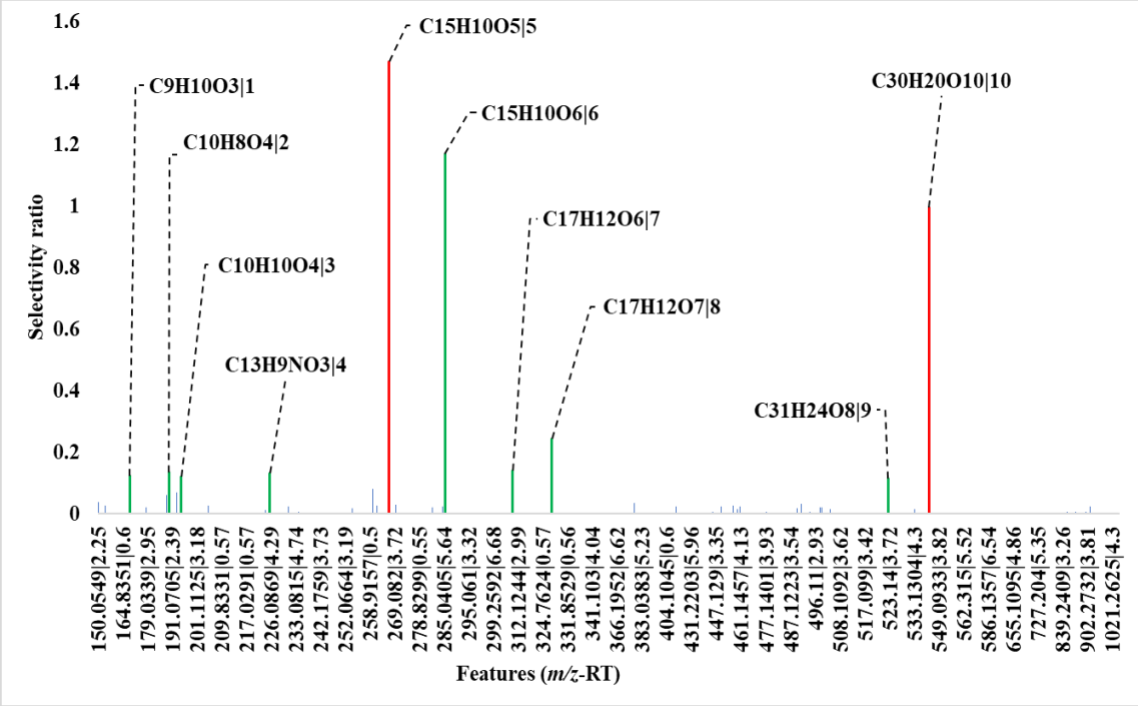

Figure 4.6. Selectivity ratio plot of *R. crispus* roots fractions 1-10 and extract at 100 µg × mL $^{-1}$. This plot shows the multivariate statistical analysis of the untargeted metabolomics dataset shows the features the correlate with growth inhibition. Percent growth inhibition of bacterial growth of each fraction or extract were used as the dependent variable. The x-axis represents the feature (identified by *m/z* and retention time) detected. Features are shown in order of increasing mass. Peaks are numbered to correspond with known and unknown metabolites that were detected. Higher selectivity ratio indicates stronger correlation with growth inhibition.

Conclusion

With this project, we (1) quantified the emodin in *Rumex crispus*, (2) determined the predicted the bioactivity of extract fractions based on the presence of emodin, (3) used untargeted approaches to identify additional features in the dataset associated with antimicrobial activity. This project shows that it is possible to identify and quantify emodin using UPLC-HRMS. Our findings show that emodin is not the only compound that contributes to the antimicrobial activity of *Rumex crispus*. In particular,

informatics analysis revealed that the presence of the compound omega-hydroxyemodin is also correlated with the antimicrobial activity of the *R. crispus* extract and fractions. This study suggests that a complex profile of metabolites may collectively be responsible for the antimicrobial activity of *Rumex crispus.*

Acknowledgments

This research was supported by the National Center for Complementary and Integrative Health of the National Institutes of Health under award numbers 5 T32 AT008938 (DDJJ), and R15 AT010191 (NBC, CVP). The authors thank Dr. Alexander Horswill for providing microbial strains utilized for this project.

CHAPTER V

CONCLUDING REMARKS AND FUTURE DIRECTIONS

Jones Jr., D.D., wrote this entire chapter with feedback and suggestions from Cech, N.B.

Concluding Remarks

We are excited to have developed a method that can simultaneously track growth and virulence in MRSA using mass spectrometry. The work described in Chapter II provides scientists in the drug discovery and natural products field the unique ability to do mechanistic studies of MRSA using one optimized method. However, it should be noted that other scientists should optimize the parameters and ensure that they are reproducible for the particular application of interest.

Future Directions

While we were able to make significant scientific progress, there is always more that can be done. Regarding the work described in Chapter III, we are still working to identify the 34 unknown MRSA features with major emphasis on those regulated by the quorum sensing system of *Staphylococcus aureus*. Our prediction is that these features could be unreported degraded peptides or small proteins that could be MRSA virulence factors. We are currently training undergraduate and graduate students to carry this project forward. With the work described in Chapter IV, we report that the antimicrobial activity of *Rumex crispus* can be attributed to multiple small molecules. This finding provides support to the idea that botanical medicines act by complex mechisms of action

that cannot always be tracked to sincle molecules. The work described in Chapter IV will be submitted for publication in a peer-reviewed journal. This is one of the most exciting chapters because it involved mentoring of students from underrepresented groups.

As a scientist, who has now given back to the community of scientists, I am honored that my work is out there for everyone to see, and I hope that this dissertation work gives future scientists hope and the will power to push through. Getting a Ph.D. is no easy task; it takes commitment to finish the job. Getting a science Ph.D. takes understanding that the first experiment will most likely fail, but we should always look for the lessons in failed experiments. There are still learning opportunities in every experiment. If I could give one piece of advice, do not let the science intimidate you; instead, be inspired to take the challenge head-on. One never knows what perseverance brings.

REFERENCES

1. Aminov, R.I., *A brief history of the antibiotic era: lessons learned and challenges for the future.* Frontiers in microbiology, 2010. **1**: p. 134-134.

2. Wenzel, M., *Do we really understand how antibiotics work?* Future Microbiology, 2020. **15**(14): p. 1307-1311.

3. DeLeo, F.R., Otto, M., Kreiswirth, B.N., and Chambers, H.F., *Community-associated meticillin-resistant Staphylococcus aureus.* Lancet, 2010. **375**(9725): p. 1557-1568.

4. Arvidson, S. and Tegmark, K., *Regulation of virulence determinants in Staphylococcus aureus.* Int J Med Microbiol, 2001. **291**(2): p. 159-170.

5. DeLeo, F.R., Otto, M., Kreiswirth, B.N., and Chambers, H.F., *Community-associated meticillin-resistant Staphylococcus aureus.* The Lancet, 2010. **375**(9725): p. 1557-1568.

6. Caesar, L.K., Kellogg, J.J., Kvalheim, O.M., and Cech, N.B., *Opportunities and limitations for untargeted mass spectrometry metabolomics to identify biologically active constituents in complex natural product mixtures.* J Nat Prod, 2019. **82**(3): p. 469-484.

7. Gordon, R.J. and Lowy, F.D., *Pathogenesis of methicillin-resistant Staphylococcus aureus infection.* Clin Infect Dis, 2008. **46 Suppl 5**: p. S350-359.

8. Thomsen, I.P. and Liu, G.Y., *Targeting fundamental pathways to disrupt Staphylococcus aureus survival: clinical implications of recent discoveries.* JCI Insight, 2018. **3**(5).

9. Otto, M., *Staphylococcus aureus toxins.* Curr Opin Microbiol, 2014. **17**: p. 32-37.

10. Sully, E.K., Malachowa, N., Elmore, B.O., Alexander, S.M., Femling, J.K., Gray, B.M., DeLeo, F.R., Otto, M., Cheung, A.L., Edwards, B.S., Sklar, L.A., Horswill, A.R., Hall, P.R., and Gresham, H.D., *Selective chemical inhibition of agr quorum sensing in Staphylococcus aureus promotes host defense with minimal impact on resistance.* PLoS Pathog, 2014. **10**(6): p. e1004174.

11. Dou, J.L., Jiang, Y.W., Xie, J.Q., and Zhang, X.G., *New Is Old, and Old Is New: Recent Advances in Antibiotic-Based, Antibiotic-Free and Ethnomedical Treatments against Methicillin-Resistant Staphylococcus aureus Wound Infections.* Int J Mol Sci, 2016. **17**(5).

12. Otto, M., *Staphylococcus aureus toxins.* Curr Opin Microbiol, 2014. **17**: p. 32-7.

13. Gordon, R.J. and Lowy, F.D., *Pathogenesis of methicillin-resistant Staphylococcus aureus infection.* Clin Infect Dis, 2008. **46 Suppl 5**: p. S350-3599.

14. Grumann, D., Nubel, U., and Broker, B.M., *Staphylococcus aureus toxins--their functions and genetics.* Infect Genet Evol, 2014. **21**: p. 583-592.

15. Kellogg, J.J., Paine, M.F., McCune, J.S., Oberlies, N.H., and Cech, N.B., *Selection and characterization of botanical natural products for research studies: a NaPDI center recommended approach.* Nat Prod Rep, 2019.

16. Cech, N.B., Junio, H.A., Ackermann, L.W., Kavanaugh, J.S., and Horswill, A.R., *Quorum quenching and antimicrobial activity of goldenseal (Hydrastis canadensis) against methicillin-resistant Staphylococcus aureus (MRSA).* Planta Med, 2012. **78**(14): p. 1556-61.

17. Junio, H.A., Todd, D.A., Ettefagh, K.A., Ehrmann, B.M., Kavanaugh, J.S., Horswill, A.R., and Cech, N.B., *Quantitative analysis of autoinducing peptide I (AIP-I) from Staphylococcus aureus cultures using ultrahigh performance liquid chromatography-high resolving power mass spectrometry.* J Chromatogr B Analyt Technol Biomed Life Sci, 2013. **930**: p. 7-12.

18. Wilson, P.A., Meyer, I.H., Antebi-Gruszka, N., Boone, M.R., Cook, S.H., and Cherenack, E.M., *Profiles of Resilience and Psychosocial Outcomes among Young Black Gay and Bisexual Men.* 2016. **57**(1-2): p. 144-157.

19. Fields, E., Morgan, A., and Sanders, R.A., *The Intersection of Sociocultural Factors and Health-Related Behavior in Lesbian, Gay, Bisexual, and Transgender Youth: Experiences Among Young Black Gay Males as an Example.* Pediatric clinics of North America, 2016. **63**(6): p. 1091-1106.

20. Wertheim, H.F., Melles, D.C., Vos, M.C., van Leeuwen, W., van Belkum, A., Verbrugh, H.A., and Nouwen, J.L., *The role of nasal carriage in Staphylococcus aureus infections.* Lancet Infect Dis, 2005. **5**(12): p. 751-62.

21. Jenul, C. and Horswill, A.R., *Regulation of Staphylococcus aureus Virulence.* Microbiol Spectr, 2018. **6**(1): p. GPP3-0031-2018.

22. Gajdács, M., *The continuing threat of methicillin-resistant Staphylococcus aureus.* Antibiotics, 2019. **8**(2): p. 52.

23. Thoendel, M. and Horswill, A.R., *Identification of Staphylococcus aureus AgrD residues required for autoinducing peptide biosynthesis.* J Biol Chem, 2009. **284**(33): p. 21828-38.

24. Thoendel, M., Kavanaugh, J.S., Flack, C.E., and Horswill, A.R., *Peptide signaling in the staphylococci.* Chem Rev, 2011. **111**(1): p. 117-51.

25. Junio, H.A., Todd, D.A., Ettefagh, K.A., Ehrmann, B.M., Kavanaugh, J.S., Horswill, A.R., and Cech, N.B., *Quantitative analysis of autoinducing peptide I (AIP-I) from Staphylococcus aureus cultures using ultrahigh performance liquid chromatography-high resolving power mass spectrometry.* J Chromatogr B, 2013. **930**: p. 7-12.

26. Todd, D.A., Zich, D.B., Ettefagh, K.A., Kavanaugh, J.S., Horswill, A.R., and Cech, N.B., *Hybrid quadrupole-orbitrap mass spectrometry for quantitative measurement of quorum sensing inhibition.* J Microbiol Methods, 2016. **127**: p. 89-94.

27. Kalkum, M., Lyon, G.J., and Chait, B.T., *Detection of secreted peptides by using hypothesis-driven multistage mass spectrometry.* Proc Natl Acad Sci U S A, 2003. **100**(5): p. 2795-800.

28. Gless, B.H., Bojer, M.S., Peng, P., Baldry, M., Ingmer, H., and Olsen, C.A., *Identification of autoinducing thiodepsipeptides from staphylococci enabled by native chemical ligation.* Nat Chem, 2019. **11**(5): p. 463-469.

29. Williams, M.R., Costa, S.K., Zaramela, L.S., Khalil, S., Todd, D.A., Winter, H.L., Sanford, J.A., O'Neill, A.M., Liggins, M.C., Nakatsuji, T., Cech, N.B., Cheung, A.L., Zengler, K., Horswill, A.R., and Gallo, R.L., *Quorum sensing between bacterial species on the skin protects against epidermal injury in atopic dermatitis.* Sci Transl Med, 2019. **11**(490).

30. Diep, B.A. and Otto, M., *The role of virulence determinants in community-associated MRSA pathogenesis.* Trends Microbiol, 2008. **16**(8): p. 361-9.

31. Laabei, M., Jamieson, W.D., Yang, Y., van den Elsen, J., and Jenkins, A.T., *Investigating the lytic activity and structural properties of Staphylococcus aureus phenol soluble modulin (PSM) peptide toxins.* Biochim Biophys Acta, 2014. **1838**(12): p. 3153-61.

32. Wu, X., Yang, M., Fang, X., Zhen, S., Zhang, J., Yang, X., Qiao, L., Yang, Y., and Zhang, C., *Expression and regulation of phenol-soluble modulins and*

enterotoxins in foodborne Staphylococcus aureus. AMB Express, 2018. **8**(1): p. 187.

33. Hodille, E., Cuerq, C., Badiou, C., Bienvenu, F., Steghens, J.P., Cartier, R., Bes, M., Tristan, A., Plesa, A., Le, V.T., Diep, B.A., Lina, G., and Dumitrescu, O., *Delta Hemolysin and Phenol-Soluble Modulins, but Not Alpha Hemolysin or Panton-Valentine Leukocidin, Induce Mast Cell Activation.* Front Cell Infect Microbiol, 2016. **6**: p. 180.

34. Quave, C.L. and Horswill, A.R., *Flipping the switch: Tools for detecting small molecule inhibitors of staphylococcal virulence.* Front Microbiol, 2014. **5**: p. 706.

35. Somerville, G.A., Cockayne, A., Durr, M., Peschel, A., Otto, M., and Musser, J.M., *Synthesis and deformylation of Staphylococcus aureus delta-toxin are linked to tricarboxylic acid cycle activity.* J Bacteriol, 2003. **185**(22): p. 6686-94.

36. Todd, D.A., Parlet, C.P., Crosby, H.A., Malone, C.L., Heilmann, K.P., Horswill, A.R., and Cech, N.B., *Signal biosynthesis Inhibition with ambuic acid as a strategy to target antibiotic-tesistant infections.* Antimicrob Agents Chemother, 2017. **61**(8).

37. Zimmermann, M. and Fischbach, M.A., *A family of pyrazinone natural products from a conserved nonribosomal peptide synthetase in Staphylococcus aureus.* Chem Biol, 2010. **17**(9): p. 925-30.

38. Wyatt, M.A., Wang, W., Roux, C.M., Beasley, F.C., Heinrichs, D.E., Dunman, P.M., and Magarvey, N.A., *Staphylococcus aureus nonribosomal peptide secondary metabolites regulate virulence.* Science, 2010. **329**(5989): p. 294-6.

39. Sun, F., Cho, H., Jeong, D.W., Li, C., He, C., and Bae, T., *Aureusimines in Staphylococcus aureus are not involved in virulence.* PLoS One, 2010. **5**(12): p. e15703.

40. Todd, D.A., Parlet, C.P., Crosby, H.A., Malone, C.L., Heilmann, K.P., Horswill, A.R., and Cech, N.B., *Signal Biosynthesis Inhibition with Ambuic Acid as a Strategy To Target Antibiotic-Resistant Infections.* Antimicrob Agents Chemother, 2017. **61**(8).

41. Boles, B.R., Thoendel, M., Roth, A.J., and Horswill, A.R., *Identification of genes involved in polysaccharide-independent Staphylococcus aureus biofilm formation.* PLoS One, 2010. **5**(4): p. e10146.

42. Wormann, M.E., Reichmann, N.T., Malone, C.L., Horswill, A.R., and Grundling, A., *Proteolytic cleavage inactivates the Staphylococcus aureus lipoteichoic acid synthase.* J Bacteriol, 2011. **193**(19): p. 5279-91.

43. Löfblom, J., Kronqvist, N., Uhlén, M., Ståhl, S., and Wernérus, H., *Optimization of electroporation-mediated transformation: Staphylococcus carnosus as model organism.* J. Appl. Microbiol., 2007. **102**(3): p. 736-47.

44. Nair, D., Memmi, G., Hernandez, D., Bard, J., Beaume, M., Gill, S., Francois, P., and Cheung, A.L., *Whole-genome sequencing of Staphylococcus aureus strain RN4220, a key laboratory strain used in virulence research, identifies mutations that affect not only virulence factors but also the fitness of the strain.* J. Bacteriol., 2011. **193**(9): p. 2332-5.

45. Pluskal, T., Castillo, S., Villar-Briones, A., and Oresic, M., *MZmine 2: modular framework for processing, visualizing, and analyzing mass spectrometry-based molecular profile data.* BMC Bioinformatics, 2010. **11**: p. 395.

46. Kellogg, J.J., Todd, D.A., Egan, J.M., Raja, H.A., Oberlies, N.H., Kvalheim, O.M., and Cech, N.B., *Biochemometrics for natural products research: Comparison of data analysis approaches and application to identification of bioactive compounds.* J Nat Prod, 2016. **79**(2): p. 376-86.

47. Kvalheim, O.M., Chan, H.-y., Benzie, I.F.F., Szeto, Y.-t., Tzang, A.H.-c., Mok, D.K.-w., and Chau, F.-t., *Chromatographic profiling and multivariate analysis for screening and quantifying the contributions from individual components to the bioactive signature in natural products.* Chemometr Intell Lab, 2011. **107**(1): p. 98-105.

48. Caesar, L.K., Kellogg, J.J., Kvalheim, O.M., Cech, R.A., and Cech, N.B., *Integration of Biochemometrics and Molecular Networking to Identify Antimicrobials in Angelica keiskei.* Planta Med, 2018. **84**(9-10): p. 721-728.

49. Johnson, J.G., Wang, B., Debelouchina, G.T., Novick, R.P., and Muir, T.W., *Increasing AIP macrocycle size reveals key features of agr activation in Staphylococcus aureus.* Chembiochem, 2015. **16**(7): p. 1093-100.

50. Vasquez, J.K., Tal-Gan, Y., Cornilescu, G., Tyler, K.A., and Blackwell, H.E., *Simplified AIP-II peptidomimetics are potent inhibitors of Staphylococcus aureus AgrC quorum sensing receptors.* ChemBiochem, 2017. **18**(4): p. 413-423.

51. Wilson, D.J., Shi, C., Teitelbaum, A.M., Gulick, A.M., and Aldrich, C.C., *Characterization of AusA: a dimodular nonribosomal peptide synthetase responsible for the production of aureusimine pyrazinones.* Biochemistry, 2013. **52**(5): p. 926-37.

52. Secor, P.R., Jennings, L.K., James, G.A., Kirker, K.R., Pulcini, E.D., McInnerney, K., Gerlach, R., Livinghouse, T., Hilmer, J.K., Bothner, B., Fleckman, P., Olerud, J.E., and Stewart, P.S., *Phevalin (aureusimine B) production by Staphylococcus*

aureus biofilm and impacts on human keratinocyte gene expression. PLoS One, 2012. **7**(7): p. e40973.

53. Newman, D.J. and Cragg, G.M., *Natural products as sources of new drugs over the 30 years from 1981 to 2010.* J Nat Prod, 2012. **75**(3): p. 311-35.

54. Yarovoy, J.Y., Monte, A.A., Knepper, B.C., and Young, H.L., *Epidemiology of Community-Onset Staphylococcus aureus Bacteremia.* West J Emerg Med, 2019. **20**(3): p. 438-442.

55. Rajasree, K., Fasim, A., and Gopal, B., *Conformational features of the Staphylococcus aureus AgrA-promoter interactions rationalize quorum-sensing triggered gene expression.* Biochemistry and biophysics reports, 2016. **6**: p. 124-134.

56. Todd, D.A., Zich, D.B., Ettefagh, K.A., Kavanaugh, J.S., Horswill, A.R., and Cech, N.B.J.J.M.M., *Hybrid Quadrupole-Orbitrap mass spectrometry for quantitative measurement of quorum sensing inhibition.* 2016. **127**: p. 89-94.

57. Jones, D.D., Jr., Caesar, L.K., Pelzer, C.V., Crandall, W.J., Jenul, C., Todd, D.A., Horswill, A.R., and Cech, N.B., *Targeted and untargeted analysis of secondary metabolites to monitor growth and quorum sensing inhibition for methicillin-resistant Staphylococcus aureus (MRSA).* J Microbiol Methods, 2020. **176**: p. 106000.

58. Rajalahti, T. and Kvalheim, O.M., *Multivariate data analysis in pharmaceutics: a tutorial review.* Int J Pharm, 2011. **417**(1-2): p. 280-90.

59. Rajalahti, T., Arneberg, R., Kroksveen, A.C., Berle, M., Myhr, K.-M., and Kvalheim, O.M., *Discriminating Variable Test and Selectivity Ratio Plot: Quantitative Tools for Interpretation and Variable (Biomarker) Selection in Complex Spectral or Chromatographic Profiles.* Analytical Chemistry, 2009. **81**(7): p. 2581-2590.

60. Rajalahti, T., Arneberg, R., Berven, F.S., Myhr, K.-M., Ulvik, R.J., and Kvalheim, O.M., *Biomarker discovery in mass spectral profiles by means of selectivity ratio plot.* Chemometrics and Intelligent Laboratory Systems, 2009. **95**(1): p. 35-48.

61. Kvalheim, O.M. and Karstang, T.V., *Interpretation of latent-variable regression models.* Chemometrics and Intelligent Laboratory Systems, 1989. **7**(1): p. 39-51.

62. Kvalheim, O.M., Chan, H.-y., Benzie, I.F.F., Szeto, Y.-t., Tzang, A.H.-c., Mok, D.K.-w., and Chau, F.-t., *Chromatographic profiling and multivariate analysis for screening and quantifying the contributions from individual components to the bioactive signature in natural products.* Chemometrics and Intelligent Laboratory Systems, 2011. **107**(1): p. 98-105.

63. Nakayama, J., Uemura, Y., Nishiguchi, K., Yoshimura, N., Igarashi, Y., and Sonomoto, K., *Ambuic acid inhibits the biosynthesis of cyclic peptide quormones in gram-positive bacteria.* Antimicrob Agents Chemother, 2009. **53**(2): p. 580-6.

64. Li, J.Y., Harper, J.K., Grant, D.M., Tombe, B.O., Bashyal, B., Hess, W.M., and Strobel, G.A., *Ambuic acid, a highly functionalized cyclohexenone with antifungal activity from Pestalotiopsis spp. and Monochaetia sp.* Phytochemistry, 2001. **56**(5): p. 463-8.

65. Zhou, Y., Huang, L., Ji, S., Hou, S., Luo, L., Li, C., Liu, M., Liu, Y., and Jiang, L., *Structural Basis for the Inhibition of the Autophosphorylation Activity of HK853 by Luteolin.* Molecules, 2019. **24**(5).

66. Halsey, C.R., Lei, S., Wax, J.K., Lehman, M.K., Nuxoll, A.S., Steinke, L., Sadykov, M., Powers, R., and Fey, P.D., *Amino Acid Catabolism in Staphylococcus aureus and the Function of Carbon Catabolite Repression.* mBio, 2017. **8**(1): p. e01434-16.

67. Zheng, L., Yan, M., Fan, F., and Ji, Y., *The Essential WalK Histidine Kinase and WalR Regulator Differentially Mediate Autolysis of Staphylococcus aureus RN4220.* J Nat Sci, 2015. **1**(6).

68. Chugh, N.A., Bali, S., and Koul, A., *Integration of botanicals in contemporary medicine: road blocks, checkpoints and go-ahead signals.* Integr Med Res, 2018. **7**(2): p. 109-125.

69. Song, X. and Hu, S., *Adjuvant activities of saponins from traditional Chinese medicinal herbs.* Vaccine, 2009. **27**(36): p. 4883-90.

70. Zhou, M., Zhang, R.H., Wang, M., Xu, G.B., and Liao, S.G., *Prodrugs of triterpenoids and their derivatives.* Eur J Med Chem, 2017. **131**: p. 222-236.

71. Alp Avci, G., Köse, D., Emniyet, A., Suicmez, M., and Avci, E., *In vitro antimicrobial and antioxidant activities and GC/MS analysis of the essential oils of Rumex crispus and Rumex cristatus.* Hacettepe Journal of Biology and Chemistry, 2014. **2**: p. 193-193.

72. Yildirim, A., Mavi, A., and Kara, A.A., *Determination of antioxidant and antimicrobial activities of Rumex crispus L. extracts.* J Agric Food Chem, 2001. **49**(8): p. 4083-9.

73. Eom, T., Kim, E., and Kim, J.-S., *In Vitro Antioxidant, Antiinflammation, and Anticancer Activities and Anthraquinone Content from Rumex crispus Root Extract and Fractions.* Antioxidants (Basel, Switzerland), 2020. **9**(8): p. 726.

74. Minh, T.N., Van, T.M., Andriana, Y., Vinh, L.T., Hau, D.V., Duyen, D.H., and Guzman-Gelani, C.d., *Antioxidant, Xanthine Oxidase, α-Amylase and α-Glucosidase Inhibitory Activities of Bioactive Compounds from Rumex crispus L. Root.* Molecules (Basel, Switzerland), 2019. **24**(21): p. 3899.

75. Humphries, R.M., Ambler, J., Mitchell, S.L., Castanheira, M., Dingle, T., Hindler, J.A., Koeth, L., and Sei, K., *CLSI Methods Development and Standardization Working Group Best Practices for Evaluation of Antimicrobial Susceptibility Tests.* J Clin Microbiol, 2018. **56**(4).

76. Caesar, L.K., Nogo, S., Naphen, C.N., and Cech, N.B., *Simplify: A Mass Spectrometry Metabolomics Approach to Identify Additives and Synergists from Complex Mixtures.* Analytical Chemistry, 2019. **91**(17): p. 11297-11305.

77. Kvalheim, O.M., Brakstad, F., and Liang, Y., *Preprocessing of analytical profiles in the presence of homoscedastic or heteroscedastic noise.* Analytical Chemistry, 1994. **66**(1): p. 43-51.

78. Kvalheim, O.M. and Karstang, T.V., *Interpretation of latent-variable regression models.* Chemometrics and Intelligent Laboratory Systems, 1989. **7**(1-2): p. 39-51.

79. Rebstock, M.C., Crooks, H.M., Controulis, J., and Bartz, Q.R., *Chloramphenicol (Chloromycetin).1IV.1aChemical Studies.* Journal of the American Chemical Society, 1949. **71**(7): p. 2458-2462.

80. Kellogg, J.J., Todd, D.A., Egan, J.M., Raja, H.A., Oberlies, N.H., Kvalheim, O.M., and Cech, N.B., *Biochemometrics for Natural Products Research: Comparison of Data Analysis Approaches and Application to Identification of Bioactive Compounds.* Journal of Natural Products, 2016. **79**(2): p. 376-386.

81. Sumner, L.W., Amberg, A., Barrett, D., Beale, M.H., Beger, R., Daykin, C.A., Fan, T.W., Fiehn, O., Goodacre, R., Griffin, J.L., Hankemeier, T., Hardy, N., Harnly, J., Higashi, R., Kopka, J., Lane, A.N., Lindon, J.C., Marriott, P., Nicholls, A.W., Reily, M.D., Thaden, J.J., and Viant, M.R., *Proposed minimum reporting standards for chemical analysis Chemical Analysis Working Group (CAWG) Metabolomics Standards Initiative (MSI).* Metabolomics, 2007. **3**(3): p. 211-221.

82. Başkan, S., Daut-Ozdemir, A., Günaydin, K., and Erim, F.B., *Analysis of anthraquinones in Rumex crispus by micellar electrokinetic chromatography.* Talanta, 2007. **71**(2): p. 747-50.